ABSTRACT

DESHPANDE, MONICA VIJAY. Poly(ε-caprolactone) Resorbable Knitted Auxetic Scaffolds for Craniofacial Skeletal Muscle Regeneration (Under the direction of Dr. Martin W. King).

Craniofacial microsomia is a congenital deformity caused by asymmetric development of the skull (cranium) and face before birth. Current treatments include corrective surgery and replacement of the deformed structure using autograft tissue, which results in donor site morbidity. An alternative therapy can be achieved by developing a resorbable scaffold for skeletal muscle regeneration which will help restore the symmetry and function of the facial muscles and reduce donor site morbidity. We have fabricated two sample knitted scaffolds with a unique auxetic structure, having a negative Poisson's ratio. These scaffolds exhibit their auxeticity through increase in total volume as well as no lateral narrowing when stretched longitudinally. Auxetic structures are currently being incorporated into a range of textile applications, such as architectural textiles, ballistic protection and sport textiles. This study will be one step in evaluating their advantages and limitations in this particular tissue engineering application. In order to operate in a dynamic bioreactor, the scaffold needs to incorporate an elastic and resorbable yarn with high elongation and 100 percent recovery when pulsed so as to mimic the function of smooth muscle tissue. Two prototype samples of the auxetic fabrics have been knitted from poly(ε-caprolactone) multifilament yarns using two different weft knitting designs. A number of their basic physical and mechanical properties have been measured, including thickness, total porosity, pore size distribution, bursting strength, elongation at break, the tendency to ravel and changes in the crosswise dimension and total volume when stressed. These prototype scaffold samples were then seeded with neonatal Human Dermal Fibroblasts so as to determine their biocompatibility in terms of their cell metabolic activity, cell attachment and proliferation at different time points over a time period of 7 days cell culture using alamarBlue® and live/dead stained confocal microscopy assays.

In terms of their physical characterization both scaffold samples exhibited the expected amount of total porosity and pore size distribution. Evaluation of the mechanical properties showed that the bursting strength and elongation at break of the scaffolds were sufficient and comparable to those of skeletal muscle tissue. In the biological evaluation, Fabric A showed superior cell metabolic activity and cell proliferation compared to the Fabric B. Further, we have identified future evaluation studies that will be essentially required to take these scaffold prototypes from the bench top to a clinical application.

Poly(ε-caprolactone) Resorbable Knitted Auxetic Scaffolds for Craniofacial Skeletal Muscle Regeneration

by
Monica Vijay Deshpande

A thesis submitted to the Graduate Faculty of
North Carolina State University
in partial fulfillment of the
requirements for the degree of
Master of Science

Textile Engineering

Raleigh, North Carolina
2019

APPROVED BY:

_____	_____
Dr. Martin W. King Committee Chair	Dr. Stephen Michielsen
_____	_____
Dr. Matthew Fisher	Dr. Susan Bernacki External Member

DEDICATION

To my beloved family

To my friends

To my advisor Dr. Martin W. King

BIOGRAPHY

Monica Deshpande was born on February 04, 1993 in Nagpur, Maharashtra, India. She has been studying Textiles since after her high school. She completed her Diploma in Textile Manufactures from Government Polytechnic, Nagpur, India in 2012. She graduated in 2015 with an undergraduate degree in Textile Engineering from Veermata Jijabai Technological Institute, Mumbai, India. After graduation she went back to Nagpur and she was working as a Visiting Lecturer in Somalwar Nikalas Mahila Mahavidyalaya in the academic year 2015-16. She taught three courses including Apparel & Non-apparel Textiles, Fundamentals of Knitting Technology and Technical Textiles to B.Sc. Textile Science second year and third year students.

In 2016 Fall, she came to North Carolina State University for pursuing her Master of Science in Textile Engineering. She is one of the members of Dr. Martin W. King's Biomedical Textiles research group. She is also a member of Society for Biomaterials and serves as Treasurer in the Society for Biomaterials student chapter at North Carolina State University.

Her mother is an Electrical Engineer, currently working as Deputy Executive Engineer in Chandrapur Super Thermal Power Station, MAHAGenco, Maharashtra, India. Monica is determined to be a professor in her home country India along with continuing her research. Hence, she wants to pursue Ph.D. after her Masters. Besides research she also maintains her interest in music in singing. She is learning Indian classical music from age five. Her other hobbies include reading Marathi, English novels, playing musical instruments such as harmonium, violin and playing outdoor games.

ACKNOWLEDGMENTS

I would like to sincerely thank my advisor Dr. Martin W. King, for constantly supporting and encouraging me throughout my masters' project. He has been a great mentor and inspiration through his continuous motivation, patience and enthusiasm. I consider myself very fortunate to be able to work with him and learn a lot from him in research. His immense knowledge and guidance have helped me in all the time of research and writing this thesis.

I would also like to extend my gratitude towards Dr. Michielsen, Dr. Fisher and Dr. Bernacki for agreeing to be a part of my advisory committee, who have inspired and supported me during my research. My sincere thanks to Dr. Shah, Assistant Professor at the UNC Chapel Hill, for introducing me to this interesting project, and helping and guiding me throughout completion of my research. I also wish to thank Dr. West for helping me out in the knitting experiments. My sincere thanks to the researchers and technicians who have helped me through my project: Dr. Xiaoyan Luo, Dr. Lauren Katz, Mr. Jeff Krauss, Dr. Nelson Vinueza and his research group members, Ms. Teresa White, Mr. Geoffrey Scott, Mr. Tim Pleasants and Mr. Tri Vu. I would also like to thank to thank all the members of my BMT research group for their constant support. Special thanks to Dr. Hui Cong and Dr. Yu Xie for helping me with my experiments.

Last but not the least I want to express my gratitude to my beloved parents for believing in me: My mother Mrs. Shubhangi Deshpande and my grandparents Mr. Shashikant Amle and Mrs. Shyamala Amle. Without their love and kind support this work would not have been possible. Lastly, I want to thank all my friends at NC State for accompanying me in this journey.

.

TABLE OF CONTENTS

LIST OF TABLES

LIST OF FIGURES

CHAPTER 1: INTRODUCTION

1.1. Motivation and Significance

Craniofacial microsomia is a disease which affects approximately 1 in every 5,600 children. Not only does it create a structural deficiency, but it also hinders the child's aesthetic development, such as facial expressions and appearance [1,2]. This deformity in children can be treated by corrective reconstructive surgery where the deformed jawbones and facial structure is repaired and the gap is then filled up with a muscle graft, which has the tensile and biological properties similar to the native healthy tissue. Such muscle grafts can be obtained either by removal of a muscle from the patient itself, which results in the drawback of scar formation or by tissue engineering. This latter approach provides a successful therapy to treat the same disease by avoiding the risk of donor site morbidity, but it includes engineering artificial tissue in the laboratory by using biocompatible textile structures as tissue engineering scaffolds [3,4].

Dr. Rishma Shah has worked earlier with Glass fiber-ECM tissue engineering scaffolds to evaluate their ability to provide in-vitro assistance for engineering and regeneration of craniofacial skeletal muscle [3]. A facial muscle needs to have a higher extension and flexibility than that can be obtained from a glass fiber scaffold. Thus, present study provides an alternative approach for the fabrication and evaluation of a resorbable textile structure that will provide the required physical, mechanical and biological properties in order to be used as a tissue engineering scaffold for the regeneration of craniofacial skeletal muscle.

1.2. Objectives

The ultimate goal behind this study is to fabricate a biocompatible and bioresorbable scaffold for regeneration of smooth skeletal muscle which will be used in facial muscle reconstruction surgery in order to treat craniofacial microsomia. This study is just a small step

towards achieving the above goal. This study includes the fabrication of a textile scaffold and evaluation of its properties. In order to determine whether they are favorable for *in-vitro* regeneration of facial skeletal smooth muscle, the following specific aims of the study are proposed.

1. To design a highly porous textile scaffold by knitting resorbable elastomeric multifilament yarns, to obtain up to 90 percent total porosity in order to provide optimum space for cells to attach, reside and grow to regenerate a skeletal muscle tissue *in-vivo.*

2. To fabricate a dimensionally stable scaffold using auxetic geometry in a weft knitting design. The auxetic geometry will be determined by the tendency of the knitted structure to not ravel and not to show lateral contraction, shrinkage or narrowing when stretched longitudinally. The auxeticity of this geometry will be observed by recording the change in total volume when the scaffold is stretched in one direction. The reason for using an auxetic geometry is because the ultimate objective is to use a dynamic bioreactor for mechanical stimulation of the muscle precursor cells and to regenerate a muscle tissue *in-vitro.* At this point the scaffold is not expected to change its lateral dimension when cyclic loading is applied in the longitudinal direction, in order not to expose the cells residing within the scaffold to strains other than in the longitudinal direction.

3. To design and fabricate a scaffold with strength and elasticity comparable to that of skeletal muscle, along with a load-elongation curve similar to that of skeletal muscle tissue, such that it can sustain the mechanical stresses *in-vivo* and perform as an extracellular matrix for the regeneration of skeletal muscle tissue.

4. To demonstrate the biocompatibility of the scaffold when cultured with neonatal Human Dermal Fibroblast cells. The biocompatibility of the scaffold will be determined by looking at the cell

metabolic activity and the cell attachment and proliferation of the scaffold at a number of fixed time points during 7 days of cell culture.

1.3. Outline of the thesis

The above-mentioned objectives have been undertaken and are reported through a systematic thesis as outlined here. The thesis comprises of five chapters. The first chapter of the thesis, the introduction, includes the motivation and significance of the project towards fabricating and evaluating a biocompatible textile scaffold to regenerate craniofacial skeletal muscle. Further, this chapter includes the specific objectives of the project and the ultimate goal of the study. The second chapter is the review of literature. In this chapter the physiology of the facial skeletal muscle, the need to regenerate this tissue, the current clinical approaches and possible research areas have been studied and reviewed. The third chapter describes the materials and methods used in this study. This chapter summarizes the materials used in this project and the steps taken for fabricating and evaluating the scaffolds. This chapter also gives the details of the parameters used while performing various mechanical and biocompatibility tests. The fourth chapter describes the results and discussion. In this chapter the results obtained from the physical, mechanical and biological evaluations of the scaffolds have been discussed. The fifth and the last chapter presents the conclusions and future work. In this chapter, the summary of the results obtained and the full or partial accomplishments of the objectives are described along with possible future work is proposed.

CHAPTER 2: REVIEW OF LITERATURE

2.1. Craniofacial Microsomia

Figure 2.1: Range of deformities in patients suffering from Craniofacial Microsomia. [4]

Craniofacial microsomia is a congenital disease which refers to all types of abnormalities which lead to improper growth of the skull (cranium) and face before birth. Microsomia means small organs or body structures. Most of the patients suffering from craniofacial microsomia are affected with abnormal development or growth of tissues on either or both sides of their faces as shown in Figure 2.1 [1]. Clinical abnormalities in cases of patients with craniofacial microsomia include hearing problems related to abnormal or insufficient growth of the ear and other functional challenges including swallowing, breathing and feeding problems. Psychological problems include aesthetics due to an asymmetric facial appearance, which may lead to social issues such as status, relationships, quality of life and personal acceptance [1,2]. The causes of the disease are yet unknown, but it is believed to be the result of genetic problems during development of the embryo [1].

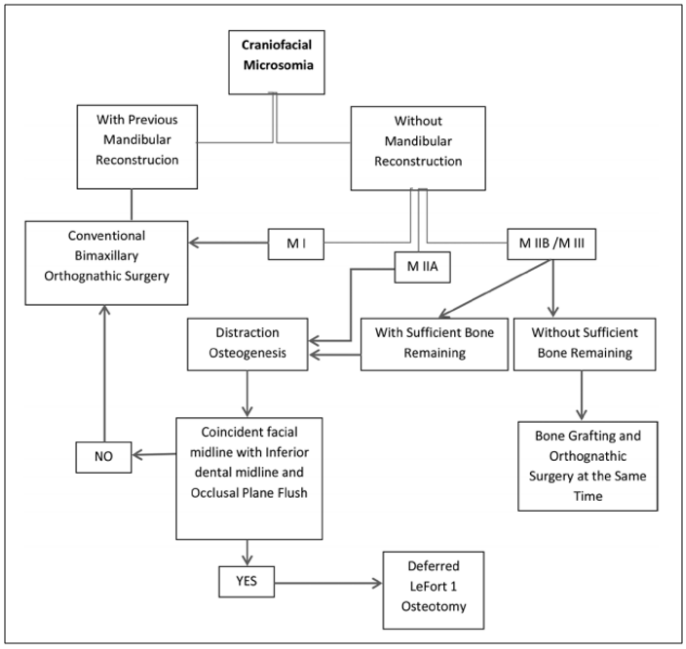

Figure 2.2: Different types and combinations of surgeries involved in treatment of Craniofacial Microsomia. [3]

Patient	Age (y)	Sex	Type of CFM, Side	Previous Reconstructed Mandibular Ramus	Mandibular Distraction Osteogenesis and Deferred Le Fort I	Bone Grafting and Orthognathic Surgery at the Same Time	Conventional Orthognathic Surgery	Follow-up
1	40	Female	MIIA, bilateral	No	X			5 y
2	33	Female	MIIA, bilateral	No	X			4 y
3	31	Male	MIIA, left	No	X			8 y
4	28	Male	MIII, right	No	X			9 y
5	18	Female	MIIA, right MIII, left	No	X			1 y
6	17	Female	MIII, right	No		X		8 y
7	17	Female	MIII, left	No		X		4 y
8	16	Female	MIIB, right	Yes			X	2 y
9	16	Male	MIII, right	Yes			X	2 y
10	15	Male	MIIA, left	No	X			3 y
11	15	Male	MIII, left	No		X		1 y
12	31	Male	MIII	No	X			5 y
13	28	Female	MIIA, right	No	X			6 mo
14	15	Male	MIIA, right MIII, left	No	X			6 mo
15	17	Female	MIIA	Yes			X	6 mo

Figure 2.3: Chart showing requirement of unique combination of corrective surgeries by individual patients based on their condition of Craniofacial Microsomia. [3]

The treatment comprises the reconstruction of craniofacial muscles in order to restore the functions along with restoration of the visual deformities. Four procedures listed in the chart in figure 2.2, namely reconstruction of mandibular ramus, mandibular distraction and osteogenesis, bone grafting and orthognathic surgery are generally involved in the treatment of CM. The combination and sequence of the procedures mainly depends on the specific conditions and extent

of defects in individual patient at the time of surgery, as shown in figure 2.3. The main procedure involved is the corrective surgery of jaw which is called as orthognathic surgery. Following the distraction and correction of jaw, muscle tissue grafts are required to fill in the gaps for reconstruction of the facial parts, mainly by suturing to either muscle or tendon depending upon local pathology [3]. The muscle tissue grafts can be obtained from either biological grafts such as free flap or fat grafts but it increases the risk of graft rejection and has a drawback of donor site morbidity in case of requirement of a large amount of tissue [4]. Sufficient muscle graft availability can be satisfied by a tissue engineered muscle graft which has several advantages such as reduction in rejection of tissue as autologous cells from the patient can be used and availability of tissue in required amount [3].

Several biomaterial-based tissue engineering approaches have been developed during recent years. For example, a bioresorbable glass fiber-collagen composite scaffold has been developed for craniofacial skeletal muscle regeneration. There are several advantages of using a biomaterial scaffold for tissue engineering over the use of biological grafts. These include the flexibility of the scaffold, the ability to engineer the required structural, physical, and mechanical properties, the ability to adjust resorption rates and the absence of donor site morbidity and scar formation [5].

2.2. Tissue Engineering

Tissue engineering is an interdisciplinary therapy which combines the principles and techniques of engineering and life sciences for the fundamental understanding of the structure-function relationships of living tissues and organs in the development of living biological substitutes for the augmentation or replacement of diseased or injured tissues [6]. Tissue

engineering is an approach which involves the in-vitro regeneration of various types of tissues, such as skin, bone, tendon, cardiac, ligament, vascular and nerve tissues in order to achieve significant improvement in the quality of life of the patient [7]. Cells, scaffolds and growth-stimulating signals are the three sides and key components of tissue engineering. Scaffolds are generally polymeric biomaterials and their main function is to provide a structural support for the cells to adhere, migrate and proliferate [8].

2.3. Skeletal Muscle Regeneration

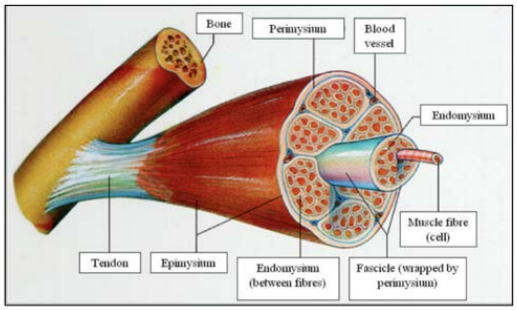

Figure 2.4: Structure of skeletal muscle. [5]

Skeletal muscles enable and control precise movements of parts of the human anatomy (Figure 2.4). According to the literature it is estimated that there are around 640 or more skeletal muscles in the human body which comprise approximately 35 percent of the total body mass [9]. The functional unit of a skeletal muscle is a long cylindrical muscle fiber or myofibril, which undergoes contraction to generate force in the axial direction. Each myofiber is composed of myofibrils which incorporate thousands of sarcomeres. The sarcomeres are composed of actin and myosin filaments which interact with each other to generate the force. Myofibers are multinucleated, and they consist of hundreds of myonuclei which are formed from the fusion of many myoblasts during the development of an embryo. Studies have shown that skeletal muscles have a robust regenerative capacity *in-vivo* that enables an injured skeletal muscle to undergo rapid

reestablishment of full power in a period of three weeks. Even after repeated injuries, a skeletal muscle continues to regenerate thousands of myoblasts [9].

2.4. Satellite Cells

Satellite cells are responsible for generating myoblasts during postnatal skeletal muscle regeneration. These satellite cells reside in a cavity on the surface of the myofibers and beneath the sheath of the basal lamina. Satellite cells can provide homeostasis to the muscle fiber. Satellite cells can also undergo cell division for muscle regeneration and provide myoblasts for muscle growth, and as the muscle matures, they can again become mitotically quiescent. Satellite cells also possess a high potential for self-renewal so as to maintain their own population, which is one of the characteristics of stem cells. It has been reported that a single isolated satellite cell can also produce many donor derived satellite cells. The donor cells themselves are capable of muscle regeneration, and also the donor derived cells participate in muscle recovery after transplantation. Hence satellite cells can be called muscle resident myogenic stem cells [9].

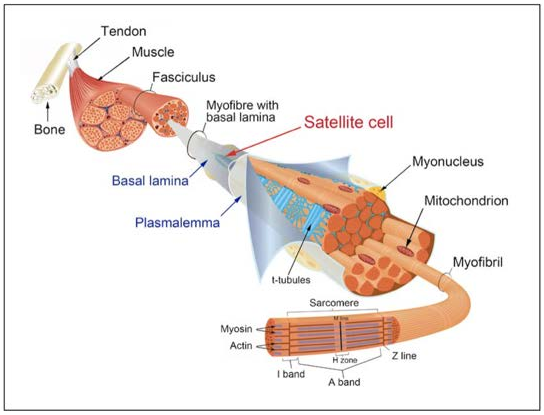

Figure 2.5: Structure of skeletal muscle and the location of satellite cells. [9]

Satellite cells have been found to be heterogeneous in nature. For instance, their characteristic features like proliferation rate and differentiation rate vary amongst satellite cell populations from different muscles as well as from the same muscle. It has been demonstrated

from various studies that a high rate of proliferation is not a common feature amongst satellite cells. Experiments studying their proliferation have shown that implanted grafts rarely generate large numbers of new satellite cells. At the same time, it has been demonstrated experimentally that an absence or loss of satellite cells results in retarded growth or loss of function of skeletal muscle, which can be characterized by muscle weakness and other deformities such as craniofacial microsomia. Though many other cell populations have also been studied for their potential to regenerate myoblasts, Relaix and Zammit have shown that satellite cells are essential for myofiber growth and muscle regeneration [9].

2.5. Scaffolds in Tissue Engineering

Biomaterials used as scaffolds for tissue engineering applications need to perform several functions such as the need for support of cellular components and providing a surface for cell adhesion, migration and proliferation. The scaffolds also need to have an open porous structure with a high level of total porosity and a large surface area to volume ratio so as to achieve a high cell density. The scaffold should provide the required mechanical strength, physical properties and dimensional stability. It should also degrade at an optimum rate to enhance the growth and orientation of the newly formed tissue which will increasingly contribute to supporting the applied mechanical forces. Biocompatible polymeric scaffolds present a number of advantages in order to meet these various functions. The risk of morbidity is reduced. The polymer composition and scaffold structure can be engineered to achieve the required properties and architecture to mimic the original tissue being replaced, to ensure better function and improve aesthetics. Certain growth factors need to be added to encourage cell migration, growth and tissue development [10]. The availability of a variety of biodegradable or bioresorbable biomaterials is advantageous because repeat surgery for the removal of the scaffold after healing is not required [11].

2.6. Textiles as Scaffolds

Textile structures are often used as scaffolds for tissue engineering applications and the design of other medical devices. This is because textile structures offer a unique combination of properties that are essential for accomplishing various scientific functions. The advantages of using textile structures as scaffolds are as follows [11].

- Different types of resorbable fiber forming polymers are available, where each polymer exhibits a different set of physical, mechanical and chemical properties such as crystallinity, elasticity and rate of resorption.
- Textile structures, in their various forms such as fiber, yarns and fabrics, provide the initial strength and flexibility, along with variations in thickness and light weight, to support the tissue development.
- Textiles provide a significantly high amount of total porosity which encourages cell attachment, growth and proliferation.

Knitted textile structures such as warp knitted and weft knitted fabrics have been studied and found to be favorable as scaffolds for tissue engineering mainly because of their interlocked loop structure these fabrics provide high amount of total porosity and also high elasticity and stretch recovery as compared to other traditional textiles, namely woven and nonwoven fabrics.

In previous research, different weft and warp knitted textiles have been studied as scaffolds for *in-vitro* regeneration of different tissues. Such as, different designs of 100% Polyester and polyester/spandex weft knitted fabrics have been studied for regeneration of cardiac tissue [12]. Weft knitted fabrics have also been studied extensively for tissue engineered vascular grafts. For

example, a recent study included fabrication and evaluation of bilayer collagen vascular graft incorporating circular weft knitted structure [13]. Warp knit structures have also been studied for applying in tissue engineering as scaffolds [14].

The following section lists various bioresorbable polymers that are available and can be used in the construction of tissue engineering scaffolds. The physical properties of the different polymers are listed below in Table 2.1 [11].

Table 2.1: Physical properties of bioresorbable polymers. [11]

Polymer name	Melting temperature (Tm)	Glass transition temperature (Tg)	Crystallinity	Time for strength loss	Time for mass loss
Poly(glycolic acid)	224 - 230 ^{O}C	36 - 40 ^{O}C	45 - 55%	1 - 2 months	4 - 12 months
Poly(lactic acid)	170 - 180 ^{O}C	55 - 65 ^{O}C	37%	6 - 12 months	24 - 66 months
Poly(ε-caprolactone)	55 - 60 ^{O}C	- 60 ^{O}C	Semicrystalline	-	24 - 36 months
Polydioxanone	106 - 115 ^{O}C	-10 - 0 ^{O}C	55%	1 - 2 months	6 - 12 months

- Poly(glycolic acid): PGA is an aliphatic poly(-ester), being one of the first bioresorbable polymers developed for biomedical applications. PGA is highly crystalline and hence has superior stiffness and dimensional stability. The degradable polymer loses its strength in 1 to 2 months, while its mass takes significantly longer to resorb, usually 2 to 4 years. PGA has been studied extensively in short-term tissue engineering applications, such as scaffolds for bones, tendon, cartilage, as well as spinal and dental regeneration. PGA is utilized less as a homopolymer but more often as a copolymer with other resorbable polymers so as to reduce the degree of crystallinity and enhance the rate of resorption [11].

- Poly(lactic acid): PLA is a widely used and researched biomaterial for resorbable medical device design. PLA displays outstanding biocompatibility along with superior mechanical properties such as high strength and modulus, thermal processability and it can be obtained from renewable natural sources like corn. PLA can be obtained in three different stereoisomeric forms such as poly-L-lactic acid (PLLA), poly-D-lactic acid (PDLA), and the copolymer of the two isomers, poly-DL-lactic acid (PDLLA). PLLA is the naturally occurring isomer, which is a semicrystalline polymer having a high melting point. Due its high modulus, i.e. high strength with low elongation, it is applied in more load-bearing applications, such as scaffolds for ligament regeneration and orthopaedic reconstructions [11].

- Poly(lactide-co-glycolide): PLGA copolymers are commercially used for manufacturing various sutures and tissue engineering skin grafts. The strength and resorption rates of PLGA copolymers can be purposely engineered to meet the desired performance. Higher proportions of lactide increase the rate of hydrolysis while higher proportions of glycolide improve the mechanical properties. PLGA copolymers are amorphous biopolymers with glass transition temperatures between 40 and 60 degree Celsius and they degrade by bulk erosion [11].

- Poly(-caprolactone): PCL is a semicrystalline elastomeric biopolymer with low tensile strength, but high elongation at break; usually greater than 300%. The PCL polymer degrades at a slow rate and takes around 2 to 3 years for total resorption. Thus it is usually blended or copolymerized with other biopolymers such as poly(lactic acid) and poly(glycolic acid). PCL copolymers are being used commercially to manufacture monofilament sutures and drug delivery devices [11].

- Polyhydroxyalkanoates: These are linear aliphatic polymers synthesized by bacteria as storage compounds for energy. Different polymers are found in this group with a wide range of resorption rate. These polymers are characterized by a high degree of polymerization and a high molecular weight. Poly-3-hydroxybutyrate (P3HB) and poly-4-hydroxybutyrate (P4HB) are two of the most commonly studied polymers in the class of PHAs. P3HB is stiff, rigid and brittle, and has an ultimate strength around 40 MPa and 6 percent elongation at break. In comparison, P4HB is a more ductile and flexible polymer which has an ultimate tensile strength of 104 MPa and up to 1000% elongation at break. These polymers degrade by surface erosion and their bioresorption rates vary widely between 2 to 12 months. The bioresorption rate depends on various factors such as their chemical composition, surface area, molecular weight and degree of crystallinity. P3HB and P4HB fibers have found applications as sutures, while their nonwoven webs have been studied as nerve repair conduits. P3HB scaffolds have been studied for spinal cord and bone regeneration, while P4HB multifilament yarns have been studied as vascular grafts, patches, scaffolds, ligaments and hernia repair meshes [11].

- Polydioxanone: PDO is a glycolide derived bioresorbable polymer which claims superior flexibility due to the introduction of poly(ether-ester) linkages. An increase in the ether linkages adds to the flexibility, while an increase in ester linkages increases the rate of degradation. For example, flexible and thicker PDO monofilament sutures and hernia repair meshes have been evaluated and are recommended clinically to overcome the higher risk of infection when using PLA and PGA multifilament sutures and meshes [11].

- Poly(trimethylene carbonate): PTMC is the only studied and used biomedical polymer in the class of polycarbonates. It is a flexible, elastomeric and slow degrading polymer with

a Tg at -17 degree Celsius. Being an amorphous homopolymer at body temperature, PTMC finds few biomedical applications due to its inferior mechanical properties. PTMC copolymers with PLA, PGA and other resorbable polymers, however, show better mechanical behavior and a higher rate of degradation compared to the homopolymer [11].

- Polyurethanes: Thermoplastic polyurethanes (TPUs) are known for their superior biocompatibility and mechanical properties. Hence, they have been incorporated into implantable medical devices such as vascular grafts and cardiac pacemakers. However, their limited long term biostability restricts their clinical use to bioresorbable implantable devices [11].

- Poly(ester amides): These polymers contain both an amide and ester linkage. The amide group gives good thermal and mechanical properties, whereas the ester group provides faster bioresorption via a hydrolytic mechanism. These polymers have been applied in the fabrication of resorbable sutures [11].

2.7. Auxetic Fabrics

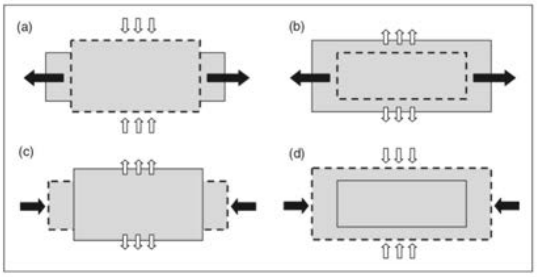

Figure 2.6: Stretch and compression in auxetic structures (b & d), as opposed to conventional structures (a & c). [16]

The Poisson's ratio of a material can be defined as the negative ratio between lateral strain and longitudinal strain. Most materials normally tend to shrink in the perpendicular or width direction when stretched in the longitudinal or lengthwise direction. As a result, they have a

positive Poisson's ratio. On the other hand, auxetic materials are those types of materials which have a negative Poisson's ratio. This means that they exhibit lateral shrinkage when compressed longitudinally and lateral expansion when extended or stretched longitudinally (Figure 2.6) [15]. If the volume of such materials is measured in their relaxed state and in compressed or expanded state, an increase in total volume will be observed from relaxed to extended state and a decrease in total volume from relaxed to compressed state. In other words, if a three-dimensional material exhibit change in volume as mentioned above, it can be considered as an auxetic material. There are a variety of naturally occurring auxetic materials found in nature, such as skin, ceramics, graphite, metals and zeolites. These natural auxetic materials are utilized in applications such as sensors, molecular sieves and separation filters because they have well defined molecular size cavities [16].

Due to the negative Poisson's ratio, auxetic materials possess exceptional properties such as a higher shear modulus, higher fracture toughness, indentation resistance, and a higher capacity to absorb energy [17]. To capitalize on these properties, various man-made auxetic materials and structures are being designed, fabricated and evaluated. Polyurethane foam was the first man-made structure studied for its auxetic properties. Subsequently, auxetic polytetrafluoroethylene (PTFE) and auxetic ultra high molecular weight polyethylene (UHMWPE) were developed. Auxetic composites were developed for utilizing and evaluating their superior Young's modulus. In particular, carbon/epoxy laminates were one of the earliest designs. Various auxetic textile fibers, yarns and fabrics have also been developed. The first auxetic fiber was polypropylene (PP). It was developed and studied by Alderson et al. using a continuous partial melt extrusion process. Subsequently, auxetic polyesters and auxetic nylons were developed. Auxetic yarns were designed and developed from non-auxetic fibers by winding two filaments with different levels of stiffness

helically around each other. These yarns exhibit auxetic properties even when woven into fabrics and made into composites [17]. Knitting was found to be a better fabrication process than weaving for making auxetic fabrics due to its initial flexibility in structure and design potential. Hu and Liu developed the first auxetic weft knitted fabrics on electronic flat knitting machines [15]. Glazzard and Breedon designed auxetic weft knitted fabrics using a purl rib structure with arrowhead geometry in a chevron shape [15]. Warp knitted auxetic fabrics were also developed by Ugbolue using re-entrant hexagonal structures and incorporating highly elastic yarns which were more suitable for open mesh structures [15]. Verma developed auxetic nonwoven structures using post processing methods which exhibited auxetic properties in the thickness direction [15].

Auxetic materials are designed using one of the following types of auxetic structural geometries [16].

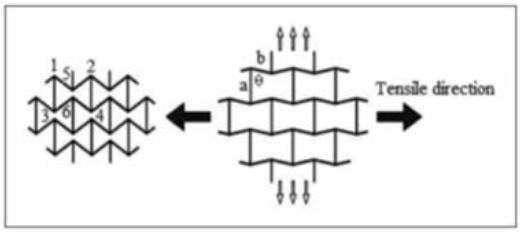

Figure 2.7: Re-entrant hexagonal auxetic structure. [16]

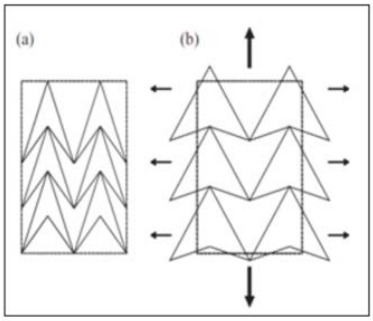

Figure 2.8: Re-entrant triangular double arrow-head auxetic geometry. [18]

1. Re-entrant auxetic structures: This structure is the most commonly used auxetic design (Figure 2.7). Two dimensional (2D) re-entrant hexagons were the first of their kind to be

studied. On longitudinal extension, these hexagons expand laterally due to the rotation of their diagonal ribs. A re-entrant honeycomb structure was also developed by Masters and Evans [16]. Other re-entrant structures include double arrowheads, which expand by opening when stretched, star shaped structures which expand by rotating ribs, and sinusoidal ligament structures which expand by opening up re-entrant cells [16]. Figure 2.8 shows one such triangular double arrowhead auxetic geometry which was studied and incorporated in warp knit structures by Alderson et al [18].

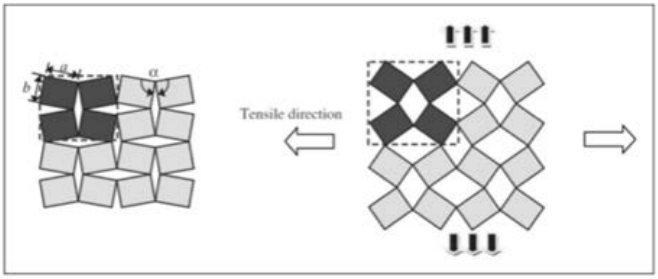

Figure 2.9: Rotating rectangle auxetic structure. [16]

2. Rotating auxetic structures: In this geometry, uniform or non-uniform units of similar or different sizes and shapes are arranged together and connected at their vertices. These units rotate and open up to expand in all directions when the structure is stretched in one direction (Figure 2.9). Grima and Evans first found these rotating auxetic structures in inorganic crystalline materials, after which they designed different rotating auxetic geometries, such as rotating squares, rotating triangles and rotating rectangles [16].

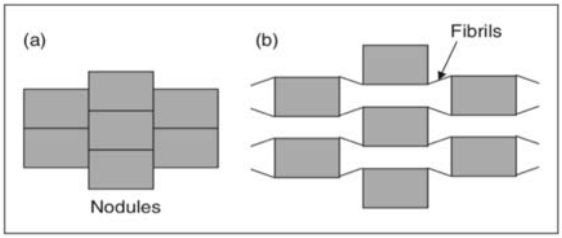

Figure 2.10: Nodule and fibril auxetic structure. [16]

3. Nodule and fibril auxetic structures: A two-dimensional (2D) model of a nodule and fibril structure was first reported by Caddock and Evans using an auxetic microporous polymer (Figure 2.10). Lim and Acharya then designed a three dimensional (3D) hexagonal model using a similar nodule and fibril structure. These structures open up in the lateral direction due to straightening of the fibrils surrounding the nodules when stretched in the longitudinal direction. It was found that these 3D structures show superior auxetic properties compared to the 2D structures [16].

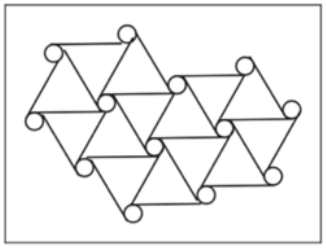

Figure 2.11: Chiral form of auxetic structure. [16]

4. Other structures incorporating auxetic geometries include chiral structures (Figure 2.11) and rod reorientation structures. Chiral structures function by wrapping and unwrapping of ligaments around rotating nodes, whereas rod reorientation structures expand in all directions due to the rotation of their rods when stretched due to being connected at specific sites [16].

Auxetic materials find applications in a number of different sectors. For example, porous auxetic materials can be used in filters as the pores will expand and open when the material is stretched. Auxetic materials exhibit limited changes in bulk properties, and so can be incorporated in sensors like hydrophones. Auxetic materials can also be used in the aerospace industry, where they serve the role as fan blades, turbine vanes, nose cones and wing panels. Biomedical applications of auxetic materials include spinal implants, annuloplasty prostheses that control the size of a heart valve annulus, artificial blood vessels and esophageal stents. Auxetic textile

structures also find applications in a wide range of uses. Auxetic fiber reinforced composites exhibit a reduced tendency of failure due to fiber pull-out compared to the use of conventional fiber reinforced composites. Woven curtains, which incorporate auxetic helically wound yarns exhibit a superior blast proof performance. Auxetic structures are also introduced in medical textiles for wound dressings and bandages. These bandages carry wound healing agents that are released when the wound swells and the bandage is stretched. Then, when the swelling goes down, the tension is reduced, the pores close and the wound healing agent is no longer released. Overall, auxetic fabrics possess improved energy absorption, resistance to indentation and shape fitting. These properties allow them to be utilized in protective clothing such as sportswear for riding, racing and skating. Auxetic textile fabrics can also be utilized in maternity wear and children's apparel as they can expand with changes in size, but do not shrink [16].

2.8. Tissue Engineering For Craniofacial Reconstruction – History of Approaches

Previous attempts in the reconstruction of craniofacial tissues include mostly bone tissue reconstruction by using biomaterials such as metallic or polymeric scaffolds and seeding them with mesenchymal stem cells. Though different types of cell sources are being used today, mesenchymal stem cells have been the most extensively used type of cell for craniofacial tissue engineering. This is because, during the development of the embryo, mesenchymal stem cells residing in the neural crest travel to participate in the process of craniofacial morphogenesis. After birth, the bone marrow is the major source of these mesenchymal stem cells [19]. Current therapies of oral and craniofacial reconstruction surgeries include metallic biomaterials such as platinum and other metal alloys, and synthetic materials such as polylactic-co-glycolic acid (PLGA) and polycaprolactone (PCL). PLGA is the most commonly used synthetic material because it is biocompatible, its structural and mechanical properties can be engineered, and its rate of

degradation can be designed and predicted. Nanospheres and microspheres of PLGA and polyglycolic acid (PGA) and often used for controlled drug delivery during craniofacial reconstruction. PLGA and polyethylene glycol (PEG) composites are also used [20]. Synthetic bioresorbable polymers are preferred over metal implants because they dissolve in body fluids and do not require a second procedure for removal as required in the case of metal implants [21]. Different techniques like injection molding have also been developed to design site specific complex geometrical scaffold shapes for the regeneration of facial cartilage tissues such as the nose and chin [22].

2.9. Design Strategies and Required Properties of Biomedical Scaffolds for Skeletal Muscle Regeneration

The use of biomaterial scaffolds over autologous grafts for skeletal muscle regeneration avoids donor site morbidity, promotes cell survival and provides better vascularization for faster healing. To achieve this, the biomaterial scaffold needs to match the morphology and mechanical properties of native tissue [23]. A biomedical scaffold has to provide control and guidance at the local level for skeletal tissue regeneration. For this, certain properties need to be considered. These properties include, total porosity, pore size distribution, biocompatibility, biodegradability, ease of fabrication, vascularization, surface topography and mechanical properties such as the tensile and compression moduli. Total porosity is essential because the higher the porosity of the scaffold, the larger the surface area which promotes cell proliferation and faster infiltration into the scaffold. High porosity is also advantageous for better cell migration and faster regeneration of the tissue. Total porosity and pore size distribution can be engineered at the time of manufacturing the scaffold. The biodegradability of the polymeric scaffold provides its main advantage over metallic scaffolds which require a second incision for removal of the implant after the construct is healed.

Any residue of foreign material inside the body for a long duration increases the chance of infection which is avoided if the scaffold material is biodegradable. Polymeric scaffolds are popular because they enable one to control the mechanical, structural and physical properties, as well as the rate of degradation. They are easy of fabricate using well established manufacturing and textile technologies. Their only disadvantage relates to their surface characteristics, which provide poor cell adhesion and no control over the attachment of cells. Studies have shown that coating a protein layer on top of polymeric biomaterials, as well as surface modifications such as the incorporation of roughness in terms of pores, grooves and pillars, can improve cell attachment to this type of synthetic biomaterial [24]. Cells require a supply of oxygen for healthy growth and proliferation. Otherwise the cells will suffer from hypoxia. The supply of oxygen depends on the distance between a cell and the nearest capillary, and the average distance that oxygen can diffuse from a capillary is approximately 150 microns. Hence, vascularization of regenerated tissue is essential, which again is governed by the total porosity and pore size distribution. Higher total porosity, along with interconnected or open pores allows for a better supply of nutrients to the center of the scaffold and thus better vascularization. The addition of certain growth factors such as vascular endothelial growth factor (VEGF) also induces and promotes vascularization within the biomaterial scaffold. At the same time, mechanical properties are required so as to retain the scaffold's structural integrity. The tensile strength and elastic modulus of the scaffold structure should match that of the native tissue. Greater total porosity and larger pore sizes may lead to a loss in strength and stability of the structure. Thus, it is desirable to limit the total porosity and pore size distribution of a scaffold in order to obtain the required mechanical properties [25].

CHAPTER 3: MATERIALS AND METHODS

3.1. Scaffold Fabrication

3.1.1. Raw materials and knitting

This study involves fabrication and evaluation of two types of scaffolds, namely PCL Fabric A and PCL Fabric B.

For the evaluation of the scaffolds for *in-vitro* regeneration of skeletal muscle, the scaffold needs to possess enough dimensional stability so that when it goes through cyclic loading and unloading in a dynamic bioreactor, it does not put compressional stress on the cells in perpendicular direction of the muscle fiber formation. In order to achieve this dimensional stability, the auxetic knitted fabric was chosen for the evaluation. To further support and enhance the elasticity of the fabric, elastomeric Poly(ε-caprolactone) multifilament yarn was selected [26].

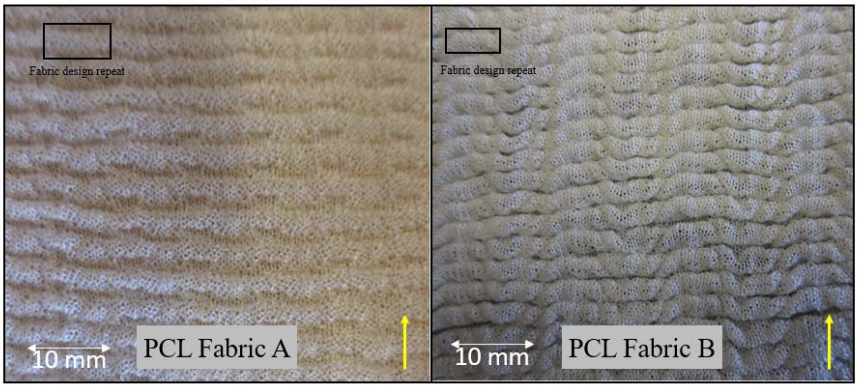

Figure 3.1: PCL A and PCL B knitted auxetic scaffold samples in relaxed state.

Poly(ε-caprolactone) (PCL) Fabric A and PCL Fabric B (Figure 3.1) were knitted from a resorbable single ply multifilament poly(ε-caprolactone) yarn with 160 denier and 36 filaments. Bobbins of PCL yarn were purchased from Guangdong Zhuhai Adhesive Products Co. Ltd., (Zhuhai, Guangdong, China). The yarn was stored in a refrigerator at 4 degrees Celsius in order to

maintain the structural changes in the bobbin to minimum, as glass transition temperature of PCL being - 60ºC.

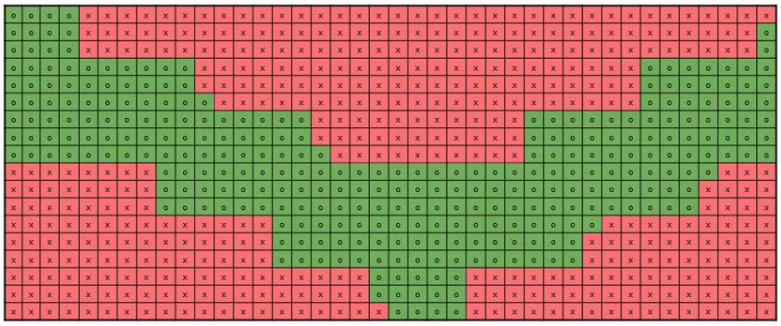

Figure 3.2: Two-dimensional view of weft rib structure design for PCL A: ‘x’(red) represents a face loop while ‘o’(green) represents a back loop.

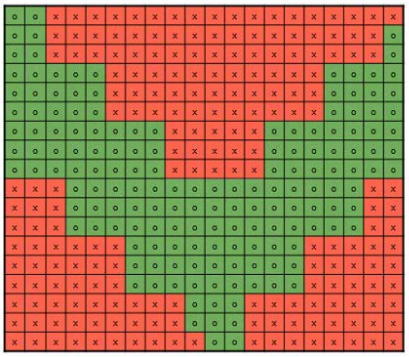

Figure 3.3: Two-dimensional view of weft rib structure design for PCL B: ‘x’(red) represents a face loop while ‘o’(green) represents a back loop.

Two different weft rib knit fabrics PCL Fabric A with 40 ends per repeat (Figure 3.2) and PCL Fabric B with 20 ends per repeat (Figure 3.3) with the same double arrowhead re-entrant auxetic geometry as mentioned in Figure 2.8 were knitted in the knitting laboratory at NC State University’s College of Textiles with the help of Dr. A. J. West. The weft knitting machine used was a Shima Seiki Model SIR123 (Figure 3.4) and the needle gauge used on the machine was gauge 18.

Figure 3.4: Shima Seiki Model SIR123 weft knitting machine at the knitting lab, Zeis Textile Extension, NC State University.

3.1.2. Cleaning and after-treatment

After knitting, the PCL Fabric A and B samples were washed thoroughly in an ultrasonic cleaning bath, also called as 'Sonicator', using distilled water and 1 gram per liter Triton-X 100 non-ionic detergent. After washing for 15 minutes, the scaffold fabrics were rinsed 3 times with distilled water at room temperature for 5 minutes each. After washing and rinsing, the excess water was removed from the fabrics with a pad mangle, which were then dried on a pin tenter frame at 30 degrees Celsius for 3 minutes in a relaxed condition. The dried samples were then heat set on a preheated pin tenter frame at 45 degrees Celsius for a 20 second dwell period.

3.2. Physical Properties

3.2.1. Total porosity

Total porosity measures the total amount of void space within a fabric structure. It is important to measure the total porosity of a scaffold in order to estimate the amount of surface area available. Higher amounts of total porosity together with an average pore size which is larger than the range of the cell sizes facilitates more cell attachment, migration, infiltration and proliferation on the tissue engineered scaffold. The total porosity of each scaffold was measured using the following standard formula:

Porosity P = 100 [A*T - W/D] / A*T

Where,

A = Area of the fabric in square centimeters

T = Thickness of the fabric in centimeters

W = Weight of the fabric in grams, and

D = Density of the fiber in g/cm^3

The thickness of the scaffold samples was measured in their relaxed state. A minimum number of 5 specimens was tested for each sample in order to obtain the average thickness for each sample. The density of the PCL fiber was considered to be 1.145 grams per cubic centimeter [27]. This value of density was used to measure the total porosity of both the scaffold samples PCL Fabrics A and B, using the above formula.

3.2.2. Pore size distribution using variable pressure scanning electron microscope

Measurement of the pore size distribution is essential to determine whether the scaffold sample is suitable for the tissue engineering application involving a specific type and size of cell. The pore size distribution was determined from SEM photomicrograph images of uncoated scaffold samples taken with a Hitachi Model S-3200 N variable pressure scanning electron microscope (Figure 3.5). The images were captured at 30 Pa pressure in a nitrogen atmosphere with an accelerating voltage of 20 kV, and magnifications in the 50x-100x range. Being highly stretchable fabric with a structure that is formed by interlocking of the face and back loops, it is difficult to measure the pore size of the weft knitted fabric in the form of a circular pore diameter. In order to standardize the procedure, the length of the pores between and/or within the yarn loops were measured, all in vertical direction. To get a statistical distribution of the pore size along with

average, 20 measurements from each image were taken manually and 5 such images of each of the samples Fabric A and Fabric B were observed.

Figure 3.5: Hitachi Model S-3200 N variable pressure scanning electron microscope at the Analytical Instrumentation Facility, NC State University.

3.2.3. Determination of auxeticity and raveling tendency:

It was necessary to confirm that the performance of the two knitted scaffold samples was indeed auxetic in nature. To demonstrate their auxeticity, two physical tests were performed. 1) The fabric should not have a tendency to ravel and 2) when the fabric was under uniaxial tensile load, it should avoid narrowing in the central width area.

Figure 3.6: Clamps used for manual testing and evaluation of raveling tendency and auxeticity of the scaffold fabric samples.

The clamps shown in the Figure 3.6 above were used to manually evaluate the raveling tendency and the auxeticity of the scaffold samples. To determine the auxeticity, the samples were cut into rectangular shaped specimens in the warp and weft directions and held in between the two clamps. The fabric specimens were stretched vertically and horizontally to determine whether they showed any lateral extension or lateral shrinkage or no change in width when stretched under tensile loading in the warp and weft directions. At the same time, it was observed whether the scaffold specimens had a tendency to ravel along the edges. The samples were stretched until they showed no lateral narrowing and the change in length and thickness was measured to determine the change in volume. Images were obtained at different extents of elongation and the auxeticity was determined.

3.3. Mechanical Properties

3.3.1. Ultimate bursting strength and elongation at break using probe puncture test method:

As the fabric samples were all weft knitted textile structures, it was necessary to measure their strength in terms of a bursting strength test rather than a tensile test method. So, in order to measure the bursting strength and elongation at break, a probe puncture test was carried out following the standard guideline ISO 7198:2016, “Cardiovascular Implants and Extracorporeal Systems. A stainless-steel puncture probe measuring 6 mm in diameter and having a smooth spherical end was used to burst the scaffold specimens held horizontally in between two flat clamping plates in a compression cage mounted on an Instron tensile tester (Figure 3.7). For the bursting strength test, 10 specimens of each scaffold sample were cut in the form of a 30 mm x 30 mm square. The load cell capacity of the instrument was 2 kN. The maximum extension was set to 26 millimeters to prevent the load cell from hitting the compression cage. The load-extension

curves were obtained using constant rate of elongation measurements at a crosshead speed of 300 mm/min.

Figure 3.7: Instron mechanical tester with the probe puncture test compression cage, used for the bursting strength and elongation tests of the knitted scaffolds.

3.4. Cell metabolic activity and Biocompatibility

Biocompatibility of PCL Fabric A and PCL Fabric B was evaluated using alamarBlue® Cell metabolic activity assays and live/dead cell viability assay with confocal microscopy. The cell metabolic activity of scaffolds samples was also compared to that of cover glass slips, considering cover glass as a favorable biomaterial for cell attachment and proliferation.

3.4.1. Sample preparation

Scaffold specimens having a circular disc shape of 13 mm diameter were stamped out of the fabrics to fit into a 24-well cell culture plate. A punch and hammer, a pair of scissors and a disposable surgical scalpel were used for the sample preparation (Figure 3.8).

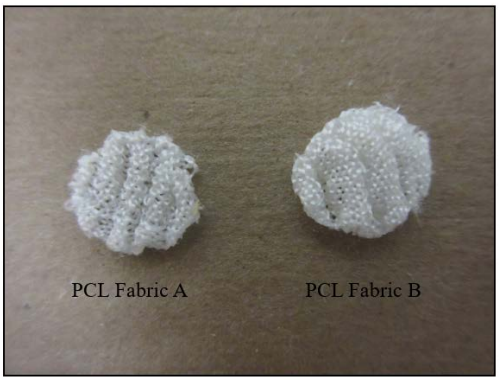

Figure 3.8: Scaffold specimens measuring 13 mm in diameter punched from PCL A and PCL B for the cell culture and biological evaluation.

3.4.2. Sterilization of the scaffolds

The scaffolds were sterilized in sterilization envelop by exposing it to ethylene oxide gas for 12 hours at ambient temperature. The sterilization was carried out at the Biomedical Engineering department at NC State University, in Auprolene Model AN74ix sterilizer (Anderson Products, Inc.). After the sterilization the scaffolds were exposed to ambient air for 48 hours for the residual ethylene oxide to evaporate from the scaffolds.

3.4.3. Cell seeding and culture

The *in-vitro* study included a 7-day cell culture experiment involving evaluation of cell metabolic activity and cell viability at day 3 and day 7. A 24-well plate (Nunclon Delta Surface, Thermo Scientific, Denmark) was prepared with 3 specimen each of round cover glass, PCL Fabric A and PCL Fabric B (Figure 3.10). The sterilized specimen were washed thrice with Posphate Buffered Solution (Gibco, Inc., Grand Island) prior to adding to the culture vessels.

From a pilot experiment carried out on glass cover slips, a seeding density of 20,000 cells per well was determined to be appropriate for the experiment in order to obtain substantial results from the alamarBlue® assays. The cell line used was male Neonatal Human Dermal Fibroblasts (Lonza, Inc., Walkersville). The cells were expanded from cryopreserved vial up to passage 3 and

harvested for the experiment (Figure 3.9). The growth medium prepared for cell culture included Dulbecco's Modified Eagle Medium (High Glucose) (Gibco, Inc., Grand Island) with 10% Fetal Bovine Serum (Speciality media, Billerica) and 1% Antibiotic Antimycotic Solution (Sigma Life Science, Israel).

Figure 3.9: Approximately 70% confluent neonatal human dermal fibroblast cells expanded in T-75 flask for seeding on the scaffolds. (100x magnification).

On day 0, the cells were seeded in 100 µL volume for each scaffold and incubated for 90 minutes prior to addition of growth medium. The working volume for each well was maintained at 500 µL. One well was seeded without any biomaterial as a positive control for alamarBlue® assay. One well was filled with only growth medium to be considered as a negative control.

One day 1, all the biomaterial specimens including cover glass and fabric scaffolds were transferred to adjacent empty wells, so that cell viability tests will include observations from only cells that have attached to the scaffolds. The cell culture was maintained in incubator for seven days along with replacing the old medium with fresh growth medium on day 3 and day 6.

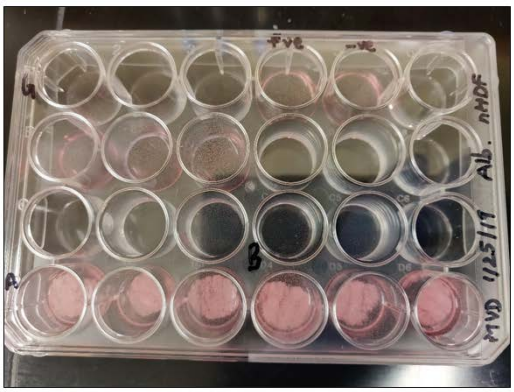

Figure 3.10: Image showing the 24-well plate including the glass cover slips and PCL scaffolds A and B seeded with neonatal human dermal fibroblast cells and fibroblast growth medium on Day 7 of the culture.

3.4.4. Cell metabolic activity using alamarBlue® assay:

The alamarBlue® assay was carried out for assessment of cell metabolic activity and proliferation without damaging the scaffold or the living cells. In this assay Resazurin dye, commercially known as alamarBlue®, which is cell permeable, non-toxic and blue in color, was used. When this non-fluorescent dye enters the cytoplasm of living cells, the metabolic activity of the cell reduces the dye to resorufin which emits a bright red fluorescence [28]. The ready-to-use alamarBlue® cell viability reagent from Invitrogen (Thermo Fisher Scientific, Oregon) was used for evaluating the cell metabolic activity on the scaffolds on day 3 and day 7 of the cell culture. The alamarBlue® reagent was thawed and directly added 50 µL to each well of the cell culture plate. 50 µL was also added to the well with only cells as positive control and well with only media as a negative control. After adding the reagent, the 24-well plate was covered with aluminium foil to reduce contact with light and incubated at 37^{o} C for 1 hour. After an hour, 3 samples of 100 µL solution from each well were taken into a fresh 96 well plate and the fluorescence was measured on Biotek model Synergy HT multi-mode microplate reader at excitation/emission wavelengths of 540/590 nm, using Gen5 software (Figure 3.11 and Figure 3.12).

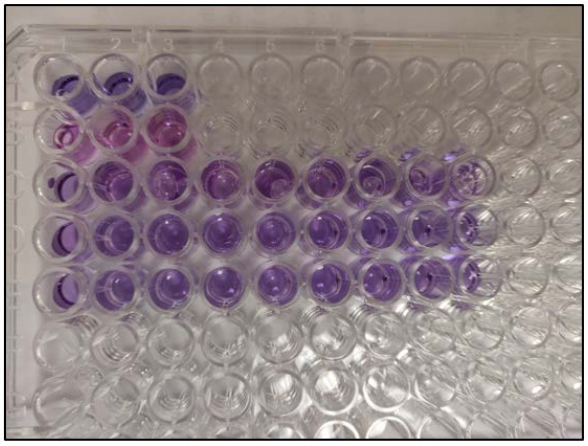

Figure 3.11: Image showing the 96-well plate for reading fluorescence in the alamarBlue® assay including 3 specimens from each of the positive and negative control and nine specimens each of the glass, PCL A and PCL B.

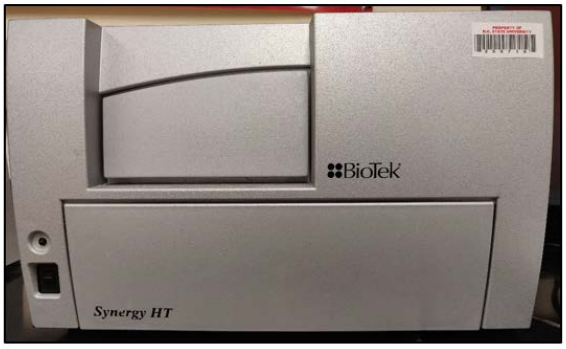

Figure 3.12: Biotek Model Synergy HT multi-mode microplate reader used for reading fluorescence with the alamarBlue® assay with Gen5 software.

3.4.5. Cell viability using live/dead staining assay and confocal microscopy:

The live/dead staining assay was carried out for assessment of cell viability and visualization of cell attachment on day 3 and day 7 of the cell culture. In this assay, a live/dead cell viability kit is used which consists of two dyes which separately stain live and dead cells in two-color fluorescence. The live and dead cells thus can be visualized simultaneously using fluorescent confocal microscopes.

The above-mentioned kit contains Calcein AM dye which is a polyanionic dye calcein, which is absorbed and retained by live cells. The intracellular esterase activity in live cells

enzymatically converts this visually non-fluorescent dye into an intensely fluorescent green stain. The second component of the kit is Ethidium Homodimer-1 (EthD-1). This dye enters the cells with damaged membranes and undergoes 40-fold increase in fluorescence on binding with nucleic acid. Thus, it produces a bright red fluorescence in dead cells but it cannot interact with the live cells due to their intact plasma membranes.

Such a live/dead viability/ cytotoxicity kit from Invitrogen (Thermo Fisher Scientific, Oregon) was obtained for the assay. This kit consists of two vials of Calcein AM, 4 mM in anhydrous DMSO, 40 µL each and two vials of EthD-1, 2 mM in DMSO H_2O 1:4, 200 µL each. A staining solution was prepared by adding 20 µL of EthD-1 and 5 µL of Calcein AM to 10 ml sterile PBS. One specimen of each of the scaffold samples was washed with PBS and the above prepared staining solution was added to each specimen in the well plate. The samples were then incubated at room temperature for 30 minutes and then images of the fluorescent cells were obtained on Zeiss model LSM 880 confocal microscope at 488 nm and 561 nm excitation wavelengths for Calcein AM and EthD-1 respectively, using Zen Black Software (Figure 3.13).

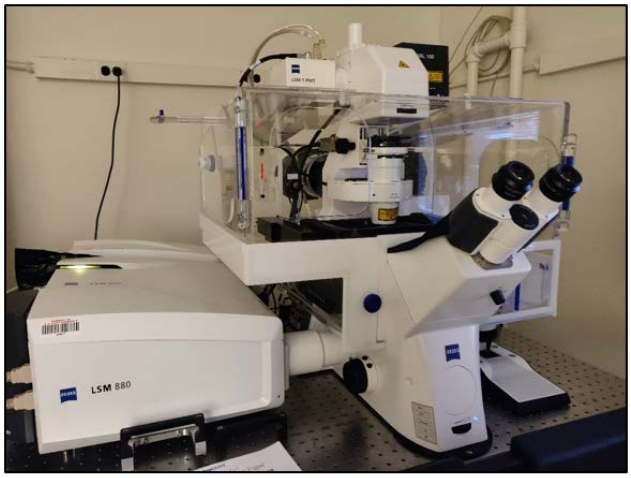

Figure 3.13: Zeiss Model LSM 880 confocal laser scanning microscope used for imaging fluorescence from live/dead assay samples with Zeiss ZenBlack software.

3.5. Statistics

The means and standard deviations were calculated for all the tests using JMP software. The two scaffold samples were compared statistically using a two-sample t-Test with unequal variances. The alpha value of 0.05 was assumed and the difference in the mean values of two samples were considered statistically significant for p values less than alpha.

CHAPTER 4 : RESULTS AND DISCUSSION

4.1. Physical Characterization of the Knitted Scaffolds

Two different types of knitted scaffold samples were fabricated from poly((ε-caprolactone) multifilament yarn by using two weft knitted fabric designs, both having auxetic geometry. The scaffold samples were named as 'PCL A' and 'PCL B' fabrics. These two samples were evaluated for application in tissue regeneration of facial skeletal muscle. The evaluation involved physical and mechanical characterization and biological tests of the two samples in order to determine the performance level of both the samples as well as comparison between the two.

The following table 4.1 includes an overview of different physical characteristics of both the scaffold samples PCL A and PCL B.

Table 4.1: Physical properties of two types of auxetic knitted scaffolds.

Scaffold Sample	No. of courses/cm	No. of wales/cm	Average fabric thickness (mm)	Fabric weight (grams/square meter)	Total Porosity (%)	Pore size range (µm)
PCL A	9	34	0.87 ±0.11	259	95	48 - 846
PCL B	14	44	1.84 ±0.07	436	94	86 - 595

The difference between the fabrications of the two samples, as mentioned in chapter 3, was that PCL A fabric consists 40 ends per repeat and PCL B consists 20 ends per repeat. Due to this difference, a difference in all the physical parameters was obtained such as number of courses and wales per centimeter were higher in PCL B than PCL A. PCL B was 1 millimeter thicker than PCL A, which reflected in the fabric weight of PCL B being almost two-fold of that of PCL A. The pore size range of PCL A was wider than that of PCL B but no significant difference was observed in the calculated total porosity of the two samples.

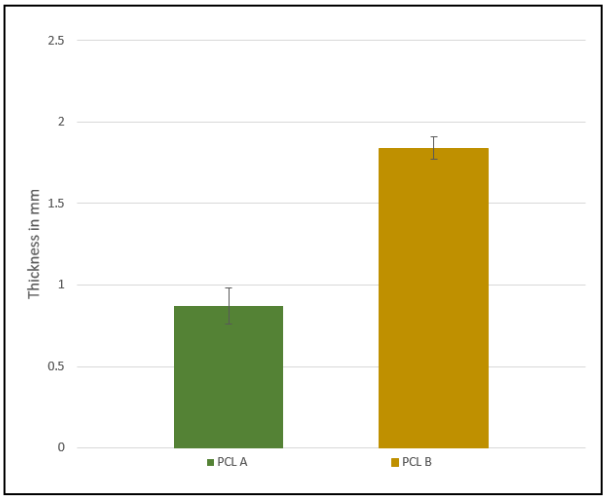

Figure 4.1: Scaffold fabric thickness in relaxed condition
(Error bars represent standard deviations).

In addition to calculating total porosity, the pore size distribution was observed for both fabric samples using a vapor pressure scanning electron microscope. The SEM images from figures 4.4 and 4.5 were used for typical pore size measurements for each fabric sample. Pores ranging in size from 48 to 846 microns were observed to be randomly distributed throughout the fabric specimens. When compared between PCL Fabric A and Fabric B, PCL Fabric A was found to have a coarser range of pore sizes with average of 319 microns whereas PCL Fabric B was found to have a finer pore size range with an average of 250 microns. The average pore sizes for both the fabrics were also statistically compared using t-Test. From the measurements, it was found that the average pore size of PCL B was significantly lower than that of PCL A. Table 4.2 shows the summary of pore size range and average pore size measurement. Figures 4.2 and 4.3 show the statistical distribution and statistical analysis of the pore size range between the two samples.

Table 4.2: Statistical summary of pore size distribution (microns) in scaffold fabric samples.

Scaffold sample	N	Range	Median	Mean	Standard deviation
PCL A	100	48 – 846	228	319	171
PCL B	100	86 - 595	282	250	117

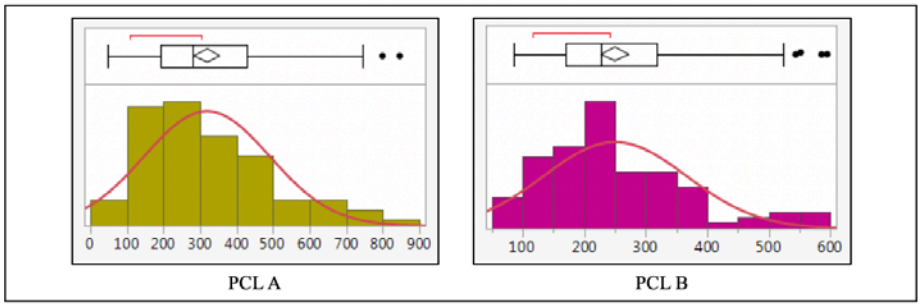

Figure 4.2: Statistical distribution of pore size range (microns) for scaffold fabric samples.

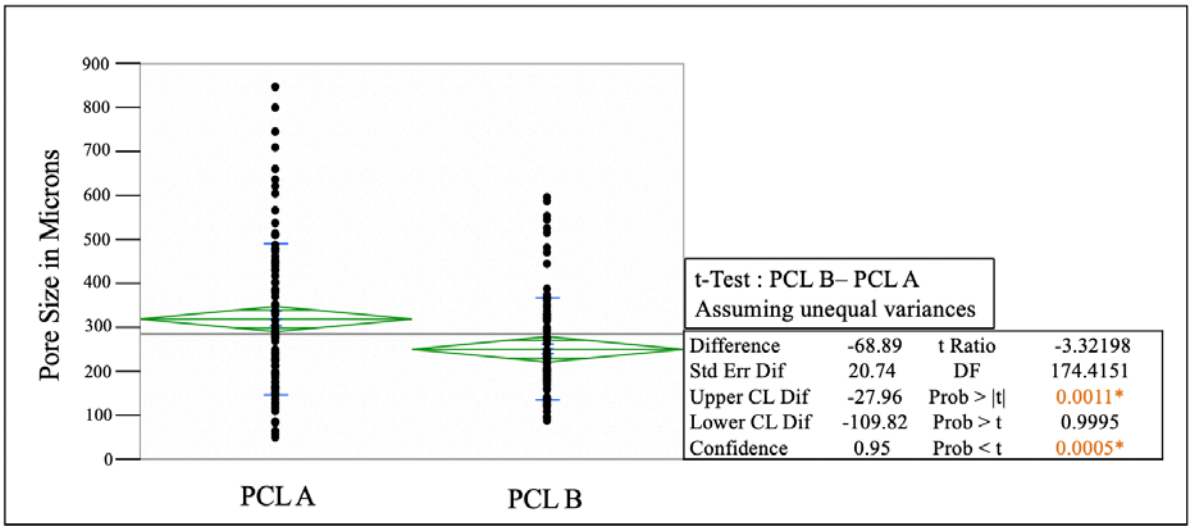

Figure 4.3: Statistical analysis of pore size distribution between PCL A and PCL B using t-Test with 0.95 confidence interval.

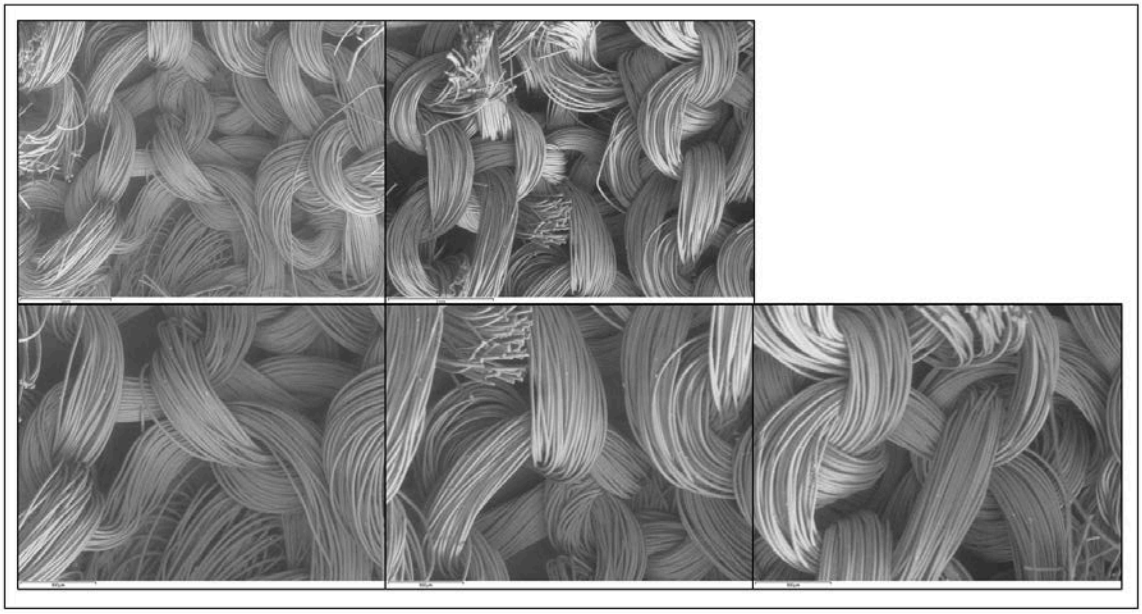

Figure 4.4: Scanning electron microscope images of PCL A.

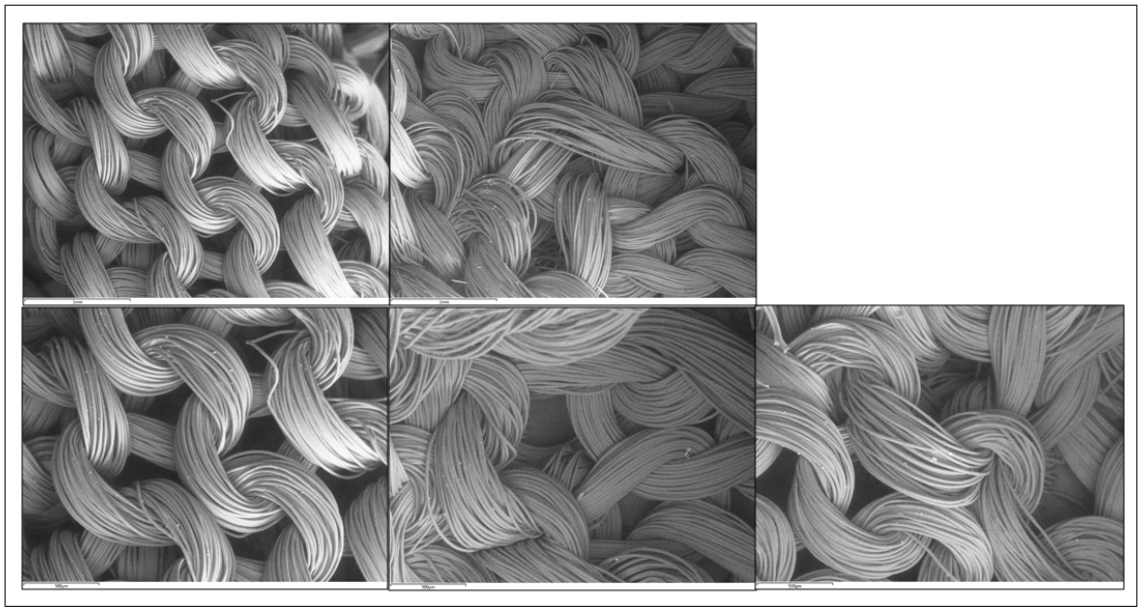

Figure 4.5: Scanning electron microscope images of PCL B.

4.2. Mechanical Properties of Scaffolds

In order to be used as a scaffold for tissue regeneration the structure needs be strong enough to sustain a load marginally higher than the original tissue to be replaced. Hence, it is important to

evaluate the mechanical properties of the scaffolds, such as ultimate tensile strength and elongation at break.

For knitted fabrics in general, it is inappropriate to measure the ultimate strength of the structure by means of the tensile strip method. This is due to the unequal distribution of load across the width of the fabric, and the narrowing of the specimen width when the specimen is under uniaxial tensile load. As a result, a probe puncture bursting test was carried out following the standard guideline test method described in ISO 7198:2016, “Cardiovascular Implants and Extracorporeal Systems”. A stainless-steel puncture probe with a 6 mm diameter smooth hemispherical end was used to burst the scaffold specimen held horizontally in between two flat clamping plates with a central open circular area measuring 12 mm in diameter. The scaffold specimens were pre-tensioned, so the crimps were removed, and the fabric was in a flat condition prior to placing them between the horizontal clamping plates. This enabled the relative bursting strengths of the two scaffold samples to be compared with each other, and with the natural tissue of the abdominal wall.

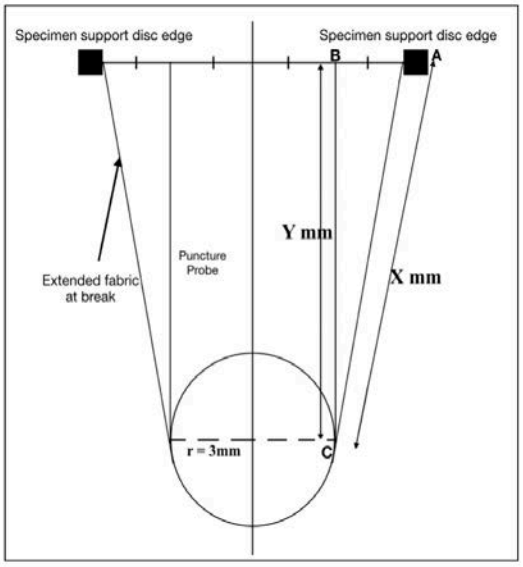

Figure 4.6: Geometric measurements of elongation at break with a compression cage using puncture probe test on an Instron tensile tester.

Considering the geometry shown in Figure 4.5, the area of the scaffold under load was taken as the area of the specimen which was under stress due to the penetration of the probe. Thus, the initial circular area of the specimen under test was the circular opening of the fabric clamps measuring 12 mm in diameter. Therefore, considering the area of a circle to be π(r^2), where r = 6 mm, then the area under load was taken to be 113.04 mm^2 and the mean bursting strength values in kPa were calculated from the average maximum load at break for each of the two samples as shown in Table 4.3 and figure 4.7.

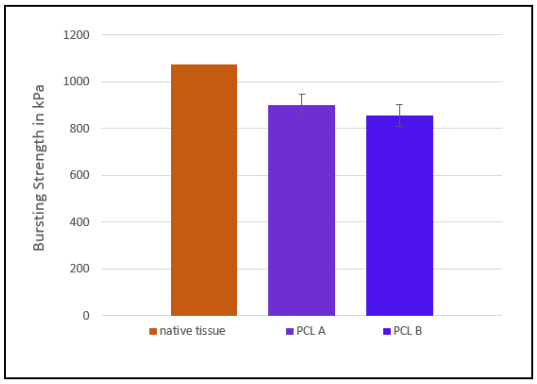

Figure 4.7: Ultimate bursting strength of scaffold samples compared to canine skeletal muscle tissue (Error bars represent standard deviations).

Table 4.3: Comparison of elongation at break and bursting strength of scaffold samples with native skeletal muscle tissue.

Scaffold Sample	Average breaking load (N)	Average bursting strength (kPa)	Average extended length (mm)	Average elongation at break (%)
Native tissue		1075		65
PCL A	102 (±5)	900 (±46)	47 (±6)	293 (±50)
PCLB	97 (±5)	856 (±48)	50 (±4)	318 (±36)

The bursting strength of a tissue engineering scaffold is expected to be slightly higher than that of the original tissue it will replace. The bursting strength of skeletal muscle tissue of rabbits is approximately 1075 kPa, while the biaxial elongation at break is approximately 65% [29]. When compared to these reference values, the two PCL fabric scaffold samples appear to be showing comparable values of average breaking strength with a standard deviation around 46 kPa. When comparing Fabric A with Fabric B, PCL Fabric A was found to have significantly higher strength than PCL Fabric B ($p < 0.05$) (Table 4.3 and Figure 4.7).

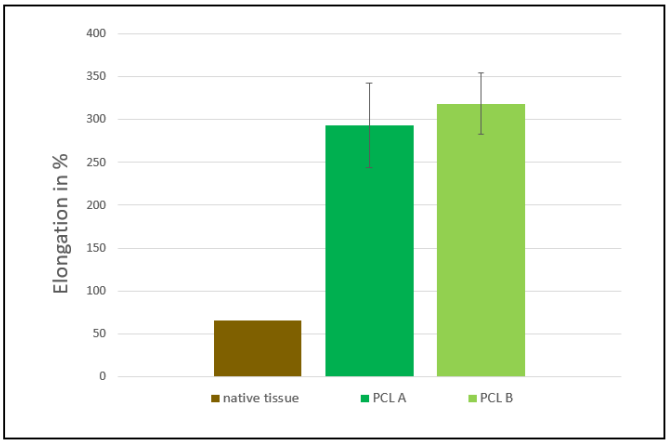

Figure 4.8: Percent elongation at break of scaffold samples compared to canine skeletal muscle tissue (Error bars represent standard deviations).

The elongation at break due to biaxial extension was calculated from the extension at break values obtained from the puncture probe bursting strength test. To calculate the linear elongation at break, the geometry shown in Figure 4.6 was used. The original length was taken as 12 mm,

which was the diameter of the open area where the specimen was held between the clamping plates. And the extended length for each specimen was calculated from the following formula:

$$\text{Extended length} = 2x + \pi r$$

where, r = 3 mm

and x is the hypotenuse of the triangle ABC in Figure 4.6. In this triangle the vertical distance y, was read from the displacement during the test.

The values of X and Y in Figure 4.6 were calculated for each specimen and the average percent extension value was obtained for the two scaffold samples. It is shown in Table 4.3 along with the standard deviation. Figure 4.8 compares the percent elongation at break values of the scaffold samples with that of the skeletal muscle tissue of rabbits. While the bursting strength values were similar to those for native muscle tissue, as mentioned earlier, the elongation at break values for both PCL scaffolds were higher than 65% which is the reference value measured for skeletal muscle tissue under biaxial loading [29]. Also, statistically no significant difference was observed in the percent elongation at break between the two samples ($p > 0.05$). This can also be seen from the biaxial stress-strain curves in Figures 4.9 and 4.10 obtained from the bursting strength test.

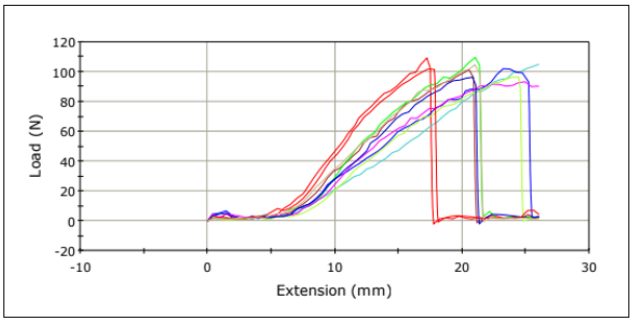

Figure 4.9: Load – elongation curves obtained from PCL A samples during bursting strength tests.

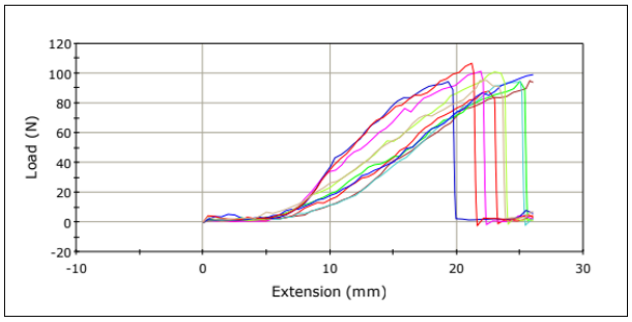

Figure 4.9: Load – elongation curves obtained from PCL A samples during bursting strength tests.

The biaxial load-elongation curve for the abdominal skeletal muscle of dogs is compared to that obtained from the bursting strength test of the scaffolds as shown in Figure 4.11. The shape of the curve with initial elongation at low stress for this reference curve is similar to that of the two PCL scaffold samples up to initial 20% elongation. It is also possible to see that the two PCL fabrics are able to mechanically support and reinforce the native muscle tissue.

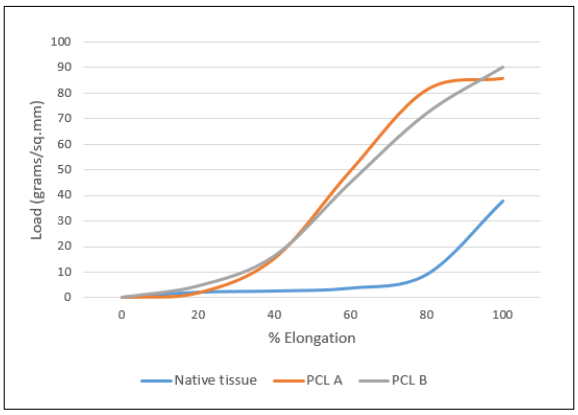

Figure 4.11: Comparison of load – elongation curves of the two scaffold samples with canine retrieved abdominal skeletal muscle tissue. [29]

4.3. Auxeticity

To measure auxeticity of the knitted scaffold structure, the fabric samples were cut into rectangular strips lying either in the warp or in the weft direction, and then subjected to a series of manually applied strain between the clamps as described earlier in Chapter 3. Figure 4.12 shows

the lengthwise stretching of the Fabric A specimen, respectively, whereas Figure 4.13 shows the lengthwise stretching of PCL B Fabric.

Table 4.4: Comparison of change in dimensions on longitudinal stretching for assessment of auxeticity in warp direction.

Scaffold samples	Before extension in warp direction				After extension in warp direction				Change in volume
	Length (mm)	Width (mm)	Thickness (mm)	**Volume (cu.mm)**	Length (mm)	Width (mm)	Thickness (mm)	**Volume (cu.mm)**	
PCL A	50	50	0.87	**2175**	88	50	0.8	**3520**	**+ 61.8 %**
PCL B	40	50	1.84	**3680**	105	50	0.76	**3990**	**+ 8.4 %**

It was observed that both the fabrics showed higher extension before perpendicular contraction in warp direction that in weft direction. This happened because the specific auxetic geometry only opens up in one direction and in the other direction the fabrics act as conventional materials. Thus in the warp direction, on manually stretching up till the fabrics showed any lateral contraction or narrowing, the dimensions of the relaxed and stretched samples in all three directions were recorded to calculate the change in volume, as mentioned in the table 4.4.

It was found that when the fabrics were stretched in warp direction, up to 76% extension for PCL A and 162% extension for PCL B, they showed increase in total volumes due to no change in width. The increase in volume was recorded to be 61.8% for PCL A and 8.4 percent for PCL B. Conventional materials having positive Poisson's ratio do not show change in volume when compressed or extended due compensation of the dimensional change in opposite direction. Here, the increase in volume for both the fabrics as a result of extension showed that these auxetic fabrics actually experience a negative Poisson's ratio, but up to a limit, which was at this stage identified to be sufficient for the desired application.

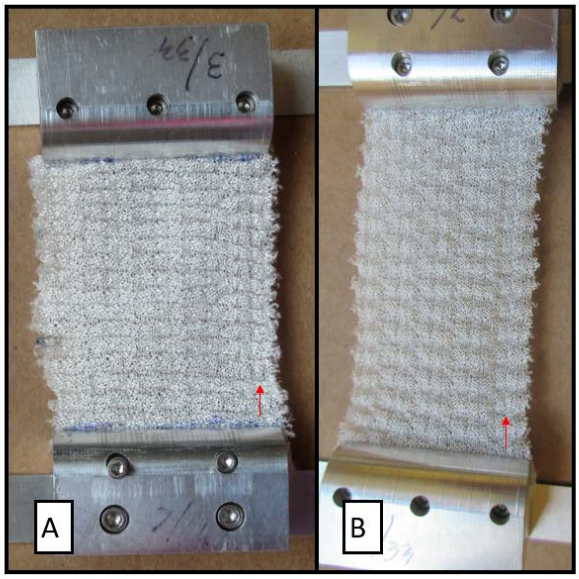

Figure 4.12: PCL Fabric A, held in clamps, showing auxeticity in warp direction A) relaxed B) stretched condition.

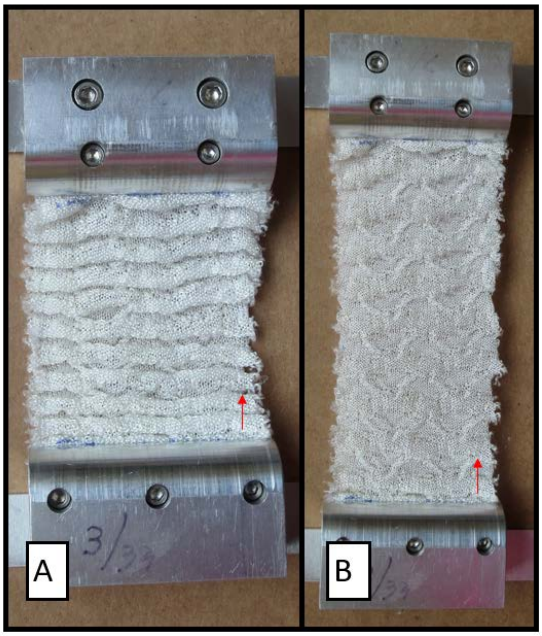

Figure 4.13: PCL Fabric B, held in clamps, showing auxeticity in warp direction A) relaxed B) stretched condition.

In addition, the scaffold samples were also observed not to ravel when stretched up to 100% under cyclic loading in a dynamic bioreactor. Normal weft knitted samples have a tendency to ravel from the finished end when exposed to such cyclic loading.

4.4. Cell Metabolic Activity and Biocompatibility

After the evaluation of the physical and mechanical properties, the scaffold samples PCL A and PCL B were evaluated for their biocompatibility. Two biological tests were carried out to evaluate the scaffolds biological response and to understand and compare their biocompatibility and their ability to regenerate specific muscle tissue. The biological tests included alamarBlue® assay for cell metabolic activity and confocal microscopy using live/dead staining assay carried out on day 3 and day 7 of the culture to determine cell attachment and proliferation on the scaffold samples.

4.4.1. AlamarBlue® assay

The results obtained from the alamarBlue® assays plate reading on day 3 and day 7 are shown in Table 4.5 and Figures 4.14-4.15. As mentioned in chapter 3, to calculate the percent reduction in each type of sample, the fluorescence from a positive control and a negative control was also obtained, which is mentioned in figure 4.15. Then, using the following formula, the percent reduction for each, the cover glass, PCL A and PCL B was calculated.

$$\%\ Reduction\ in\ sample = \frac{Sample\ fl.Value - Negative\ fl.Value}{Positive\ fl.Value - Negative\ fl.Value} \times 100$$

The percent reduction is the quantitative measure of the cell metabolic activity in the scaffolds compared to the positive control. Table 4.5 compares the percent reduction in the scaffold samples PCL A and PCL B to that in the cover glass samples and between day 3 and day 7. From

the figures, it was found that the cell metabolic activity in PCL A and PCL B was lower than that in glass samples both on day 3 and day 7. But between PCL A and PCL B, the cell metabolic activity in PCL A was significantly higher than that in PCL B ($p < 0.05$).

The reason why the average percent reduction in all the samples was as low as 10 percent on day three and 30 percent on day 7 is that all the scaffold samples were transferred from the seeding well to adjacent empty well on day 1, so that only a fraction of cells attached to the scaffolds were carried forward and were grown up to day 7. But the positive control was the culture well directly seeded with cells on day 0 and allowed to grow till day 7, which resulted into a fluorescence value for 100 percent reduction to be as high as 1272 on day 3 and 2321 on day 7, as shown in figure 4.15.

Thus, these results not only prove the biocompatibility and support from the scaffolds for cell proliferation, but also establish the capability of the scaffolds for cell attachment after seeding. As the fluorescence values of day 3 indicate from figure 4.15, when compared to positive control as well as to the glass samples, the scaffolds hold a lot of scope for improvement in cell adhesion.

Table 4.5: Comparison of per cent reduction in alamarBlue® assay on Day 3 and Day 7 between cover glass and the two scaffold samples with ± standard deviations.

Scaffold Sample	% Reduction	
	Day 3	Day 7
Glass	16 (±10)	39 (±7)
PCL A	6 (±1)	26 (±4)
PCL B	5 (±1)	19 (±3)

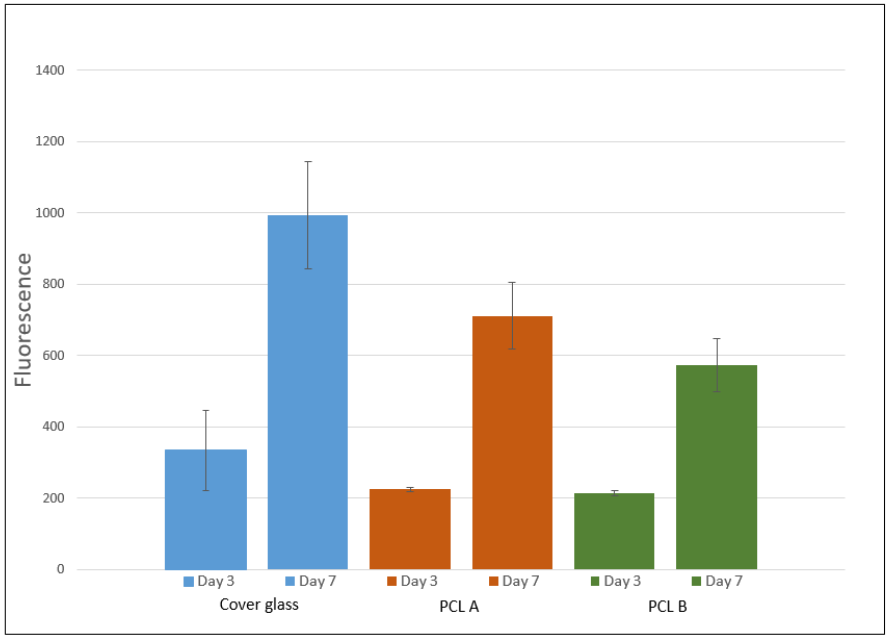

Figure 4.14: Comparison of Day 3 and Day 7 fluorescence values of the alamarBlue® assay results from the scaffold samples with those from the glass cover slips (Error bars represent standard deviations).

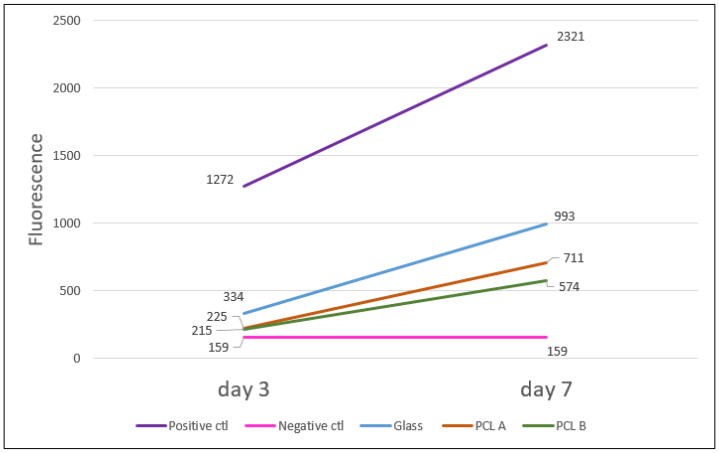

Figure 4.15: Comparison of increasing trend in fluorescence values of alamarBlue® for Day 3 to Day 7from the scaffold samples to that of the positive and negative controls.

4.4.2. Confocal microscopy with live/dead staining assay:

Figures 4.16 through 4.23 were obtained from the confocal microscopy, after staining the live cells with green fluorescent Calcein AM dye and the dead cells with EthD-1 red fluorescent dye. Images at three different fields on each scaffold specimen were obtained by scanning the scaffolds throughout the thickness on each plane at an interval of 5 microns and combined together

to visualize the residence of live and dead cells on and within the scaffold samples and compare the proportion of viable cells to the dead cells on each scaffold between day 3 and day 7 images.

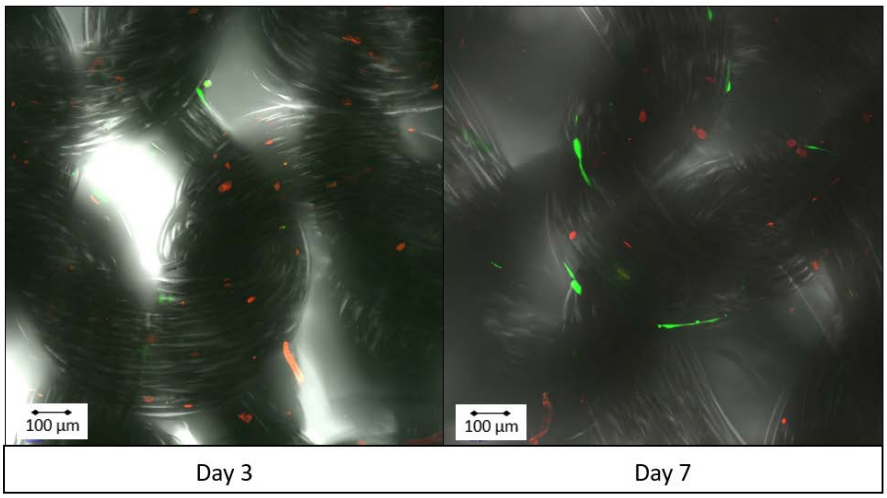

Figure 4.16: Comparison of Day 3 and Day 7 images of PCL sample A live/dead stained laser confocal microscopy with a 10x objective lens and maximum intensity projection.

Figure 4.16 shows that the cells have attached not in the pores between the yarns but within each yarn on the filaments. The fibroblasts have extended depending upon the morphology of the filament.

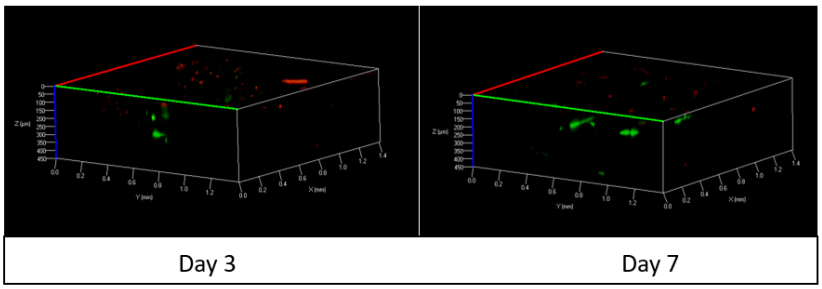

Figure 4.17: Comparison of Day 3 and Day 7 images of PCL sample A live/dead stained laser confocal microscopy with a 10x objective lens in a 3-dimensional view.

Figure 4.17 shows that the cells have migrated up to 450 microns deep into the three-dimensional scaffold, both on day 3 and day 7. This also shows that the scaffold structure and morphology helped the cells to migrate for a distance of 450 microns into the scaffold, but no

further. The depth of cell penetration in scaffolds could be the measure of either effective cell seeding or cell migration. It was difficult to interpret the exact reason, as the depth of cell penetration immediately after seeding was not visually observed.

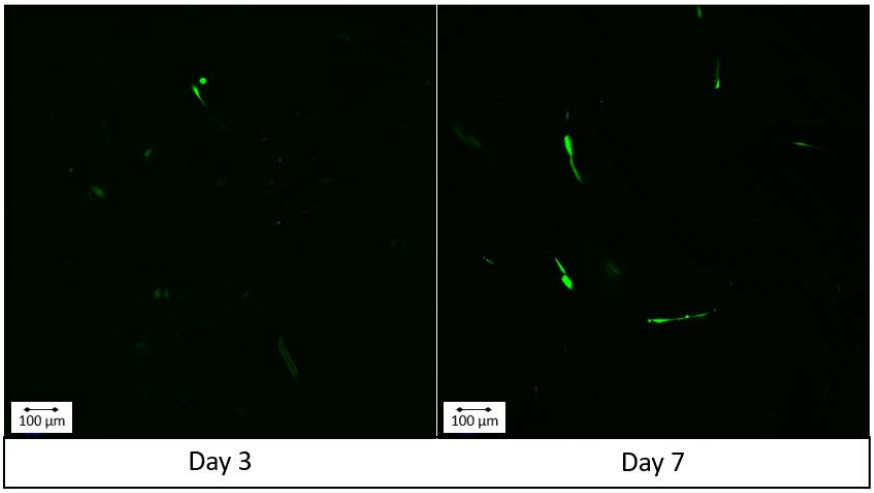

Figure 4.18: Comparison of Day 3 and Day 7 images of live cells on PCL sample A live/dead stained laser confocal microscopy with a 10x objective lens.

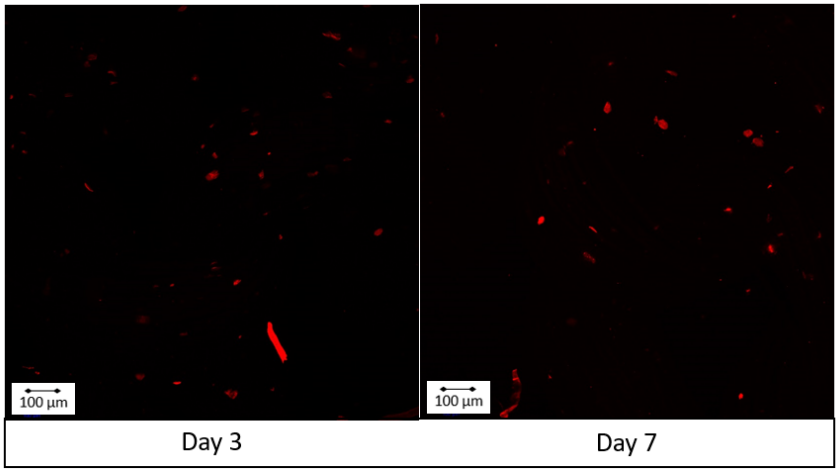

Figure 4.19: Comparison of Day 3 and Day 7 images of dead cells on PCL sample A live/dead stained laser confocal microscopy with a 10x objective lens.

Figures 4.18 and 4.19 visually compare the proportion of live and dead cells on PCL A between day 3 and day 7 of culture. From the images, it was found out that the approximate number of live cells increased from day 3 to day 7. The live cells were healthy and elongated on day 7.

There was no significant difference in the number of dead cells. It was also found that these results were supporting the results obtained from alamarBlue® assay.

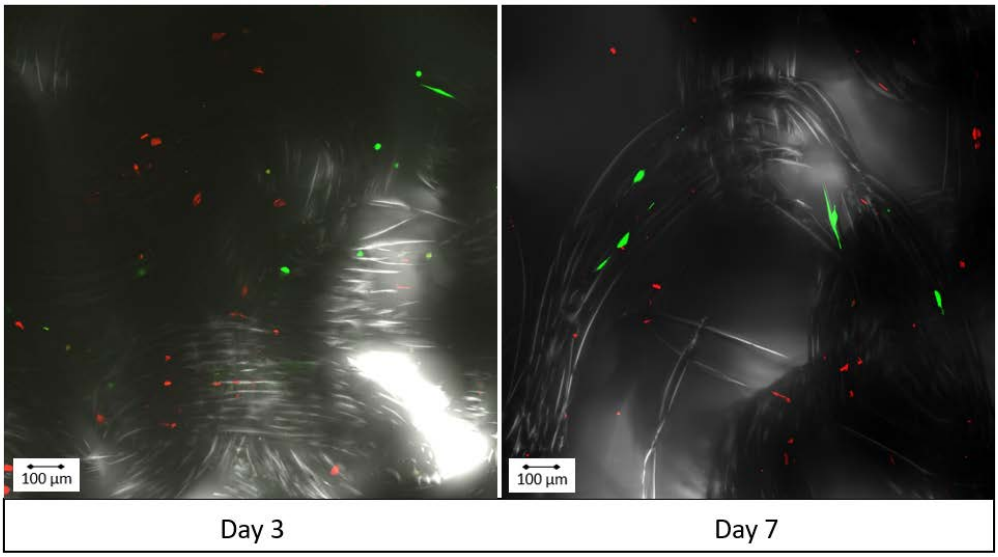

Figure 4.20: Comparison of Day 3 and Day 7 images of PCL sample B live/dead stained laser confocal microscopy with a 10x objective lens and maximum intensity projection.

Similarly, the image from PCL B samples were also obtained on day 3 and day 7 of the culture as shown in figures 4.21 to 4.23. From image 4.23 it was seen that the cells attached to the filaments in between the yarns. There was not much difference in the number of live cells as well as number of dead cells between day 3 an day 7 on PCL B, as seen in figures 4.22 and 4.23. However, the morphology of the cells compared between day 3 and day 7 shows that the cells were more healthy and elongated along the filaments on day 7 compared to day 3. From the three dimensional view of the scaffold in figure 4.21, it was found that the cells migrated to 450 microns depth on day 3 and 400 microns depth on day 7. The significance of cell penetration depth could be understood more effectively if the culture was extended further up to 14 or 28 days.

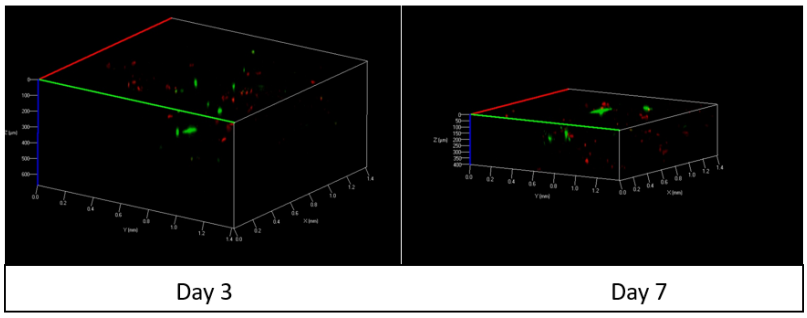

Figure 4.21: Comparison of Day 3 and Day 7 images of PCL sample B live/dead stained laser confocal microscopy with a 10x objective lens in a 3-dimensional view.

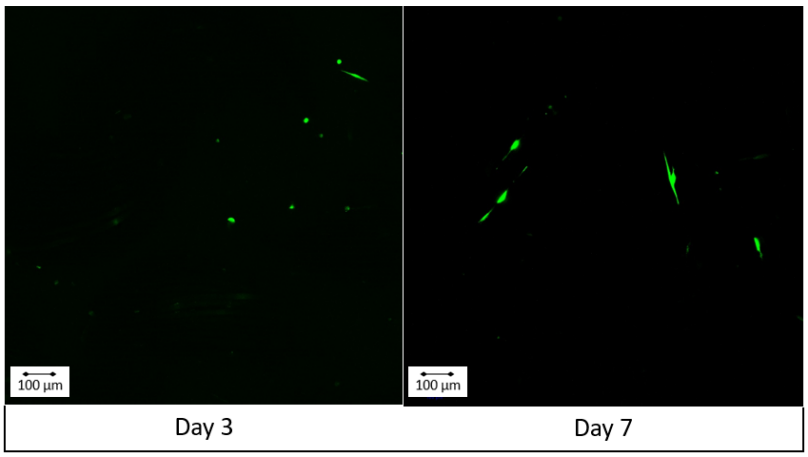

Figure 4.22: Comparison of Day 3 and Day 7 images of live cells on PCL sample B live/dead stained laser confocal microscopy with a 10x objective lens.

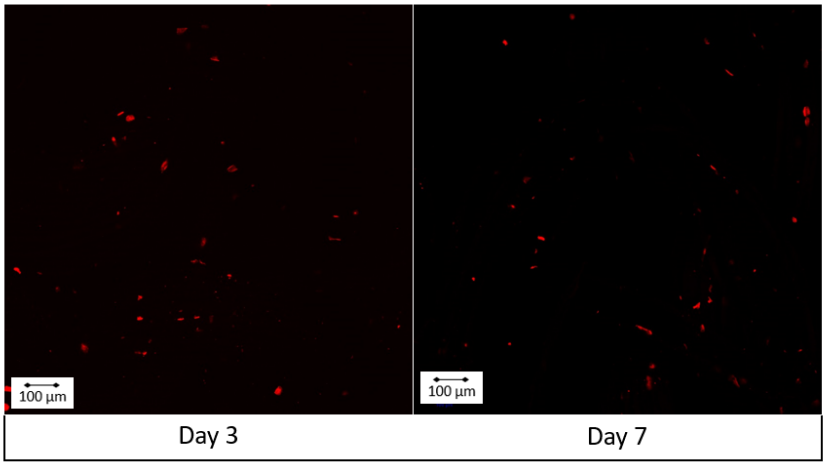

Figure 4.23: Comparison of Day 3 and Day 7 images of dead cells on PCL sample B live/dead stained laser confocal microscopy with 10x objective lens.

Figure 4.24 below is the image captured from a field with depth of 56 microns. The image shows a clearer picture of the morphology of the cells attached to the filaments of the yarn in the scaffold.

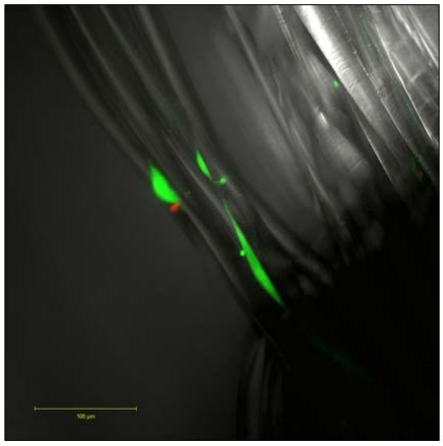

Figure 4.24: Laser scanning confocal microscopy image of PCL Fabric A with a 20x objective lens showing the attachment of cells on a single filament.

CHAPTER 5 : CONCLUSIONS AND FUTURE WORK

5.1. Conclusions

The objectives of this study were to fabricate auxetic knitted textile structures and evaluate their physical characteristics, mechanical properties and their biological evaluation such as cell metabolic activity and cell viability in order to obtain a tissue engineering scaffold which could support the regeneration of craniofacial skeletal muscle *in-vitro.*

In order to achieve a highly porous scaffold, a weft knitting approach was used to fabricate novel auxetic knitted structures using two weft rib knit designs. The two scaffold samples were then evaluated for their physical characteristics such as fabric weight, thickness, total porosity and pore size distribution. Novel auxetic geometries were used while knitting these designs on a Shima Seiki weft knitting machine. These particular geometries provided the fabrics with a negative Poisson's ratio, and as a result, the fabrics did not contract laterally along with an increase in volume observed when stretched in the longitudinal direction. This behavior is unusual for conventional textile structures. The two scaffold samples were then evaluated for their mechanical properties, such as bursting strength and elongation at break using a probe puncture test method. The auxetic behavior and tendency not to ravel were confirmed using special clamps to apply a series of strains manually.

The biological evaluation of the two scaffold samples included observation of the cell metabolic activity using the alamarBlue® assay test method. For this test, the scaffold samples were cultured *in-vitro* for 7 days with passage 3 neonatal Human Dermal Fibroblasts obtained from Lonza. The alamarBlue® test was carried out 3^{rd} and 7^{th} days of cell culture in order to compare the rate of cell metabolic activity between the two prototype scaffold samples and the cover glass sample for reference. The scaffolds were also evaluated by imaging using confocal microscopy

with live/dead staining assay on day 3 and 7 of the culture for comparing the proportion of live and dead cells between the two samples, understanding the depth in scaffolds to which the cells could migrate in 7 days, and to understand the cell attachment with respect to the morphology of the scaffold.

The results obtained from the experiments are summarized as follows:

The total porosity values for the two scaffold samples PCL Fabric A and Fabric B were calculated to be 95 and 94 percent. While the values for total porosity were on target and similar for the two samples, the pore size distribution, between the yarn loops, was significantly different between the two samples. PCL Fabric A was found to have a larger average pore size with pores in the 48 to 846 micron range compared to Fabric B, which had a smaller average pore size with pores in the 86 to 595 micron range. Also, when the SEM images were studied it was clear that the cells would not attach and reside in these open pores, as the pore size was too high as compared to the average cell size. But these open pores, which were located in between the yarns and overlapping loops, would be beneficial for the transportation of the nutrients during the cell culture.

The fabric weight in the relaxed state of the scaffold sample Fabric B was found to be higher than that of Fabric A. Likewise the thickness in relaxed state of Fabric B was higher than that for Fabric A. This was the result of the higher crimp and bulk incorporated into Fabric B due to the size of the weft knit design repeat.

The bursting strength values in kPa obtained from the experimental tests of the scaffold samples were in the same order of magnitude as the reference values for rabbit skeletal muscle obtained from the literature. Between the scaffold samples, Fabric A had a higher bursting strength than Fabric B.

It was assumed that the calculations and results for biaxial tensile elongation at break obtained from the proposed geometry were valid and comparable to the standard or reference values. Using an elastomeric yarn in a weft knitted design, both scaffold samples have been found to have an elongation at break around 300 percent, which was higher than the values found in the references. Also, the experimental load-elongation curves obtained from the samples were compared to the reference load-elongation curve for skeletal muscle of a dog. The percent elongation with respect to load applied was compared and it was found that both the scaffold samples could sustain the similar magnitude of load up to 20 percent elongation as compared to the reference curve, but after 20 percent elongation the scaffolds were much stiffer as compared to the reference skeletal muscle.

Neither of the scaffold samples was observed to have a tendency to ravel when stretched in either the length or width directions. Both the scaffold samples were found to have a higher auxeticity in the warp direction compared to the weft direction. This could be the result of the auxetic geometry which opens up in a specific direction when elongated, which imparted greater waviness, crimp and bulk in warp direction due to the particular knit designs. Also, the auxeticity was tried to determine by measuring the change in volume on application of extension force, where PCL Fabric A showed higher percent of increase in volume with no change in width as compared to PCL Fabric B. It was not yet determined why these fabrics did not extend in width as well, when elongated in longitudinal direction, as opposed to standard auxetic structures.

The cell metabolic activity results from day 3 showed that, when compared to cover glass samples, initial attachment of cells was lower on both the samples. But, the rate of increase in cell metabolic activity from day 3 to day 7 was similar in glass samples and PCL A. PCL B showed lower rate of increase in metabolism.

The confocal microscopy images supported the results obtained from the cell metabolic activity. An increase in number of live cells was visualized in PCL A while the number of live cells was equal in PCL B, between day 3 and day 7 images. The ratio of live cells to dead cells was very low in both the samples. It was also observed during microscopic evaluation that a lot of live cells detached from the samples and migrated to the staining solution. This also gave an insight to the need for improving the surface morphology of the samples for better cell attachment.

Based on the results obtained as outlined above and explained in Chapter 4, the objectives put forward in Chapter 1 can be described as follows:

1. The poly(ε-caprolactone) multifilament yarns were successfully fabricated into two different types of weft knitted textile scaffolds, PCL Fabric A and PCL Fabric B. The total porosity values thus obtained were 95% and 94% respectively. Thus the objective of obtaining a total porosity percentage higher than 90 was achieved.
2. Two types of auxetic weft knitted designs were selected, and two different scaffold samples, PCL Fabric A and PCL Fabric B were knitted. Both scaffold samples showed superior auxetic properties in the longitudinal or warp direction. This implies that when stretched lengthwise, these fabrics did not narrow down laterally. Also, neither of the scaffold samples showed a tendency to ravel. PCL A showed better auxeticity than PCL B.
3. Both scaffold samples were tested for bursting strength and biaxial elongation at break, and the results were compared with reference values obtained from skeletal muscle tissue reported in the literature. In addition, the load-elongation curves were also compared. It was found that the bursting strength values obtained from PCL Fabrics A and B were 900 and 856 kPa respectively, and they were similar to the biaxial strength of rabbit skeletal

muscle tissue, which is reported to be 1075 kPa. Also, the initial stiffness of both scaffold samples was comparable to that of the reference skeletal muscle load-elongation curve.

4. The scaffolds biological performance was measured in terms of alamarBlue® assay and live/dead assay confocal microscopy. This has enabled the cell metabolic activity, cell attachment and cell migration on both the scaffold samples to be evaluated against neonatal Human Dermal Fibroblast cells. The PCL Fabric A was found to be biologically superior compared to Fabric B in terms of cell metabolic activity over the time period of 7 day cell culture.

5.2 Future Work

Based on the conclusions and the discussion of the results with respect to the objectives, some further improvements are needed in terms of scaffold design and fabrication, test procedures and the evaluation of various properties as described below.

The pore size distribution was evaluated through images obtained from the scanning electron microscope and the cell morphology and attachment specific to scaffold structure was observed from the images obtained from confocal microscopy. The wide range of pore size distribution thus obtained in both the scaffold samples was found to be beneficial for transportation of nutrients, but the cells liked to attach on the surface of the individual or group of filaments in the yarns. Thus, there is a need to improve on fabricating scaffolds with an optimum pore size distribution which allows the transportation of nutrients but also provides more surface area for the cells to attach and migrate.

After evaluating the biocompatibility of the scaffolds for Human Dermal Fibroblasts, the obvious next step will be to evaluate whether these scaffolds support attachment and growth of facial skeletal muscle cells.

Considering the objectives and conclusions derived from the results, the following future steps need to be added to continue the project.

1. There is need to evaluate the time taken by these scaffold samples for strength loss as well as complete resorption, and compare this rate of resorption with the period of complete regeneration of a facial skeletal muscle *in-vivo*.
2. To fabricate scaffolds with an optimum pore size distribution beneficial for transportation of nutrients as well as an improved surface morphology for better cell attachment and migration.
3. To evaluate the capability of the scaffolds for skeletal muscle specific cells. If successful, the scaffolds then can be periodically strained in a dynamic bioreactor for *in-vitro* regeneration of a matured tissue.
4. It is recommended to evaluate other types of auxetic geometries as described in Chapter 2 of the literature review, for fabricating a knitted textile scaffold for regeneration of facial skeletal muscle, with favorable physical and mechanical properties.
5. The *in-vitro* regenerated tissue should then be implanted in an animal model, probably a porcine model, after the maturation of the tissue construct.
6. The level of auxeticity needs to be tested with a standard test method and apparatus. This is recommended when the scaffolds are going to be used in a dynamic bioreactor, to ensure that the applied cyclic strain falls within the level of auxeticity of the scaffold.

REFERENCES

1. Reference, G. H. (2017). Craniofacial microsomia. Retrieved from https://ghr.nlm.nih.gov/condition/craniofacial-microsomia.
2. Van de Lande, L., Caron, C., Pluijmers, B., Joosten, K., Streppel, M., Dunaway, D., Koudstaal, M., & Padwa, B. (2018). Evaluation of swallow function in patients with craniofacial microsomia: A retrospective study. *Dysphagia, 33*(2), 234-242. doi:10.1007/s00455-017-9851-x.
3. Fariña, R., Valladares, S., Torrealba, R., Nuñez, M., & Uribe, F. (2015). Orthognathic surgery in craniofacial microsomia: Treatment algorithm. *Plastic and Reconstructive Surgery Global Open, 3*(1), e294. doi:10.1097/GOX.0000000000000259.
4. Birgfeld, C., & Heike, C. (2012). Craniofacial microsomia. *Seminars in Plastic Surgery, 26*(2), 91. doi:10.1055/s-0032-1320067.
5. Shah, R. (2010). *The in vitro engineering of craniofacial muscle constructs utilising degradable composite glass fibre-collagen scaffolds*. Doctoral dissertation. Available from Dissertations & Theses Europe Full Text: Science & Technology. (ProQuest Dissertations Publishing). Retrieved from https://search.proquest.com/docview/1442496580.
6. Palsson, B., & Bhatia, S. (2004). *Tissue engineering*. Upper Saddle River, N.J.: Pearson Prentice Hall. Retrieved from http://www2.lib.ncsu.edu/catalog/record/DUKE003879540.
7. Mondal, D., Griffith, M., & Venkatraman, S. S. (2016). Polycaprolactone-based biomaterials for tissue engineering and drug delivery: Current scenario and

challenges. *International Journal of Polymeric Materials and Polymeric Biomaterials, 65*(5), 255-265. doi:10.1080/00914037.2015.1103241.

8. Chan, B., & Leong, K. (2008). Scaffolding in tissue engineering: General approaches and tissue-specific considerations. *European Spine Journal, 17*(S4), 467-479. doi:10.1007/s00586-008-0745-3.
9. Relaix, F., & Zammit, P. S. (2012). *Satellite cells are essential for skeletal muscle regeneration: The cell on the edge returns centre stage*. England: COMPANY OF BIOLOGISTS LTD. doi:10.1242/dev.069088.
10. Shah, R., & Lewis, M. P. (2010). The future? craniofacial skeletal muscle engineering as an aid for the management of craniofacial deformities. *Seminars in Orthodontics, 16*(2), 153-162. doi:10.1053/j.sodo.2010.02.008.
11. Gajjar, C. R., & King, M. W. (2014). *Resorbable fiber-forming polymers for biotextile applications* (1st ed.). Cham: Springer. doi:10.1007/978-3-319-08305-6 Retrieved from http://lib.myilibrary.com?ID=644995.
12. Chen, J. (2015). *A biodegradable knitted cardiac patch for myocardium regeneration using cardiosphere-derived cells (CDCs).* Master's Thesis, NC State University, Raleigh, USA. Retrieved From https://catalog.lib.ncsu.edu/catalog/NCSU3532801.
13. Zhang, F. (2018). *Studies of tissue-engineered vascular grafts fabricated from electro-chemically aligned collagen yarns and electrospun collagen nanofibers.* Master's Thesis, NC State University, Raleigh, USA. Retrieved From https://catalog.lib.ncsu.edu/catalog/NCSU4412856.

14. He, T. (2011). *A study of three dimensional warp knits for novel applications as tissue engineering scaffolds.* Master's Thesis, NC State University, Raleigh, USA. Retrieved From https://repository.lib.ncsu.edu/handle/1840.16/8235.

15. Wang, Z., & Hu, H. (2017). Tensile and forming properties of auxetic warp-knitted spacer fabrics. *Textile Research Journal, 87*(16), 1925-1937. doi:10.1177/0040517516660889.

16. Wang, Z., & Hu, H. (2014). Auxetic materials and their potential applications in textiles. *Textile Research Journal, 84*(15), 1600-1611. doi:10.1177/0040517512449051.

17. Ge, Z., & Hu, H. (2015). A theoretical analysis of deformation behavior of an innovative 3D auxetic textile structure. *The Journal of the Textile Institute, 106*(1), 101-109. doi:10.1080/00405000.2014.906099.

18. Alderson, K., Alderson, A., Anand, S., Simkins, V., Nazare, S., & Ravirala, N. (2012). Auxetic warp knit textile structures. *Physica Status Solidi. B, Basic Solid State Physics, 249*(7), 1322-1329. doi:10.1002/pssb.201084216.

19. Machado, E., Fernandes, M., DeSousa, P., & Gomes, H. (2012). Dental stem cells for craniofacial tissue engineering. *Oral Surgery, Oral Medicine, Oral Pathology, Oral Radiology and Endodontology, 113*(6), 728-733. doi:10.1016/j.tripleo.2011.05.039.

20. Moioli, E., Clark, P., Xin, X., Lal, S., & Mao, J. (2007). Matrices and scaffolds for drug delivery in dental, oral and craniofacial tissue engineering. *Advanced Drug Delivery Reviews, 59*(4), 308-324. doi:10.1016/j.addr.2007.03.019.

21. Shakya, A., & Kandalam, U. (2017). Three-dimensional macroporous materials for tissue engineering of craniofacial bone. *British Journal of Oral and Maxillofacial Surgery, 55*(9), 875-891. doi:10.1016/j.bjoms.2017.09.007.

22. Chang, S., Tobias, G., Roy, A., Vacanti, C., & Bonassar, L. (2003). Tissue engineering of autologous cartilage for craniofacial reconstruction by injection molding. *Plastic and Reconstructive Surgery, 112*(3), 793-799. doi:10.1097/01.PRS.0000069711.31021.94.

23. Kwee, B. J., & Mooney, D. J. (2017). Biomaterials for skeletal muscle tissue engineering. *Current Opinion in Biotechnology, 47,* 16-22. doi:10.1016/j.copbio.2017.05.003.

24. Qazi, T., Mooney, D., Pumberger, M., Geißler, S., & Duda, G. (2015). Biomaterials based strategies for skeletal muscle tissue engineering: Existing technologies and future trends.*Biomaterials, 53,* 502-521. doi:10.1016/j.biomaterials.2015.02.110.

25. Kumar, A., Nune, K., Murr, L., & Misra, R. (2016). Biocompatibility and mechanical behaviour of three-dimensional scaffolds for biomedical devices: Process–structure–property paradigm. *International Materials Reviews, 61*(1), 20-45. doi:10.1080/09506608.2015.1128310.

26. Private communication with Dr. A. J. West.

27. Xin, Y., Jianhua, L., Delin, L., & Yanpu, L. (2016). Appropriate density of PCL nano-fiber sheath promoted muscular remodeling of PGS/PCL grafts in arterial circulation. *Biomaterials, 88*, 34-47. doi:10.1016/j.biomaterials.2016.02.026.

28. alamarBlue® HS and alamarBlue® cell viability assay protocol. (2016). Retrieved from https://www.thermofisher.com/us/en/home/references/protocols/cell-and-tissue-analysis/cell-profilteration-assay-protocols/cell-viability-with-alamarblue.html

29. Yamada, H., & Evans, F. G. (1970). Strength of Biological Materials. Baltimore, Md: Williams & Wilkins.